Global Biogeochemical Cycles

RESEARCH ARTICLE
10.1029/2023GB008048

Physical Mechanisms Sustaining Silica Production Following the Demise of the Diatom Phase of the North Atlantic Spring Phytoplankton Bloom During EXPORTS

Mark A. Brzezinski[1,2], Leah Johnson[3], Margaret Estapa[4], Samantha Clevenger[5], Montserrat Roca-Martí[5,6,7], Elisa Romanelli[8], Kristen N. Buck[9], Bethany D. Jenkins[10], and Janice L. Jones[1]

[1]Marine Science Institute, University of California Santa Barbara, Santa Barbara, CA, USA, [2]Department of Ecology Evolution and Marine Biology, University of California Santa Barbara, Santa Barbara, CA, USA, [3]Applied Physics Laboratory and School of Oceanography, University of Washington, Seattle, WA, USA, [4]School of Marine Sciences, Darling Marine Center, University of Maine, Walpole, ME, USA, [5]Department of Marine Chemistry and Geochemistry, Woods Hole Oceanographic Institution, Woods Hole, MA, USA, [6]Department of Oceanography, Dalhousie University, Halifax, NS, Canada, [7]Institut de Ciència i Tecnologia Ambientals (ICTA-UAB), Universitat Autònoma de Barcelona, Cerdanyola del Vallès, Spain, [8]Earth Research Institute, University of California Santa Barbara, Santa Barbara, CA, USA, [9]College of Earth, Ocean, and Atmospheric Science, Oregon State University, Corvallis, OR, USA, [10]Department of Cell and Molecular Biology, Graduate School of Oceanography, Kingston, RI, USA

Abstract Each spring, the North Atlantic experiences one of the largest open-ocean phytoplankton blooms in the global ocean. Diatoms often dominate the initial phase of the bloom with succession driven by exhaustion of silicic acid. The North Atlantic was sampled over 3.5 weeks in spring 2021 following the demise of the main diatom bloom, allowing mechanisms that sustain continued diatom contributions to be examined. Diatom biomass was initially relatively high with biogenic silica concentrations up to 2.25 μmol Si L^{-1}. A low initial silicic acid concentration of 0.1–0.3 μM imposed severe Si limitation of silica production and likely limited the diatom growth rate. Four storms over the next 3.5 weeks entrained silicic acid into the mixed layer, relieving growth limitation, but uptake limitation persisted. Silica production was modest and dominated by the >5.0 μm size fraction although specific rates were highest in the 0.6–5.0 μm size fraction over most of the cruise. Silica dissolution averaged 68% of silica production. The resupply of silicic acid via storm entrainment and silica dissolution supported a cumulative post-bloom silica production that was 32% of that estimated during the main bloom event. Diatoms contributed significantly to new and to primary production after the initial bloom, possibly dominating both. Diatom contribution to organic-carbon export was also significant at 40%–70%. Thus, diatoms can significantly contribute to regional biogeochemistry following initial silicic acid depletion, but that contribution relies on physical processes that resupply the nutrient to surface waters.

Plain Language Summary Each spring, one of the largest phytoplankton blooms in the global ocean occurs in the North Atlantic Ocean. One group of phytoplankton, the diatoms, often dominates the early bloom. Diatoms are unique among the phytoplankton as they require the element silicon to construct their cell walls. Dissolved silicon is in relatively short supply in the North Atlantic, prompting this study of how the availability of silicic acid controls the contribution of diatoms to the bloom. At the start of our expedition, extremely low silicic acid concentrations in surface waters indicated that a diatom bloom had already occurred. Experiments revealed strong silicon limitation of the remaining diatoms. A series of four storms over 3 weeks introduced pulses of silicic acid to surface waters partially alleviating Si limitation. As a result, diatoms were able to significantly contribute to primary productivity and to the export of organic carbon despite persistent silicon limitation. The results indicate that diatoms can play a significant biogeochemical role in the North Atlantic bloom following the initial depletion of silicic acid, but their contribution is regulated by physical processes that resupply the nutrient to surface waters. Such processes may enhance overall bloom productivity and its contribution to carbon sequestration.

Key Points:

- The diatom phase of the North Atlantic spring bloom terminated due to silicon limitation
- Physical processes that reintroduced silicic acid sustained post-bloom diatom net productivity
- The resupply of silicic acid allowed Si-limited diatoms to contribute significantly to primary production and to organic carbon export

Supporting Information:

Supporting Information may be found in the online version of this article.

Correspondence to:

M. A. Brzezinski,
markbrzezinski@ucsb.edu

Citation:

Brzezinski, M. A., Johnson, L., Estapa, M., Clevenger, S., Roca-Martí, M., Romanelli, E., et al. (2024). Physical mechanisms sustaining silica production following the demise of the diatom phase of the North Atlantic spring phytoplankton bloom during EXPORTS. *Global Biogeochemical Cycles*, *38*, e2023GB008048. https://doi.org/10.1029/2023GB008048

Received 14 NOV 2023
Accepted 26 MAY 2024

Author Contributions:

Conceptualization: Mark A. Brzezinski, Margaret Estapa, Kristen N. Buck, Bethany D. Jenkins
Data curation: Mark A. Brzezinski, Margaret Estapa, Janice L. Jones
Formal analysis: Mark A. Brzezinski, Leah Johnson, Margaret Estapa, Samantha Clevenger, Montserrat Roca-Martí, Elisa Romanelli, Janice L. Jones
Funding acquisition: Mark A. Brzezinski, Margaret Estapa, Kristen N. Buck, Bethany D. Jenkins

1. Introduction

The North Atlantic spring phytoplankton bloom is one of the largest and most dramatic blooms in the global ocean, contributing significantly to global primary production and carbon export (Alkire et al., 2012;

Investigation: Mark A. Brzezinski, Leah Johnson, Margaret Estapa, Samantha Clevenger, Montserrat Roca-Martí, Kristen N. Buck, Bethany D. Jenkins
Methodology: Mark A. Brzezinski, Leah Johnson, Margaret Estapa, Elisa Romanelli, Kristen N. Buck, Bethany D. Jenkins, Janice L. Jones
Visualization: Mark A. Brzezinski, Leah Johnson, Samantha Clevenger
Writing – original draft: Mark A. Brzezinski, Leah Johnson, Margaret Estapa, Samantha Clevenger
Writing – review & editing: Montserrat Roca-Martí, Elisa Romanelli, Kristen N. Buck, Bethany D. Jenkins

Turner, 2002). Bloom dynamics in the North Atlantic are influenced by the low silicic acid to nitrate (Si:N) ratios in subsurface waters of the North Atlantic that are brought to the surface during winter mixing (Hátún et al., 2017). North Atlantic Si:N ratios are among the lowest in the global ocean at 0.5 or less (Sarmiento et al., 2004). Low Si:N interacts with other factors that also influence bloom initiation and development. The disturbance recovery hypothesis purports that the spring bloom is initiated when physical processes that deepen mixed layers lower phytoplankton mortality from grazing by diluting prey, thus lowering encounter rates (Behrenfeld, 2010; Behrenfeld et al., 2013). Others have found that the combination of increased stratification during spring following deep winter mixing promotes the development of the annual bloom (Binetti et al., 2020; Enriquez & Taylor, 2015; Rumyantseva et al., 2019). Regardless of the mechanism triggering bloom initiation, nutrient-rich waters with low Si:N ratios in the photic zone are observed at the start of the bloom. Diatoms often dominate the early stages of the bloom, especially during the positive phase of the North Atlantic Oscillation (NAO) index when silicic acid supply is enhanced by deeper winter mixed layers (Henson et al., 2012). During nutrient-replete growth that is characteristic of bloom events, diatoms are expected to consume silicic acid and nitrate in a ratio of about 1:1 (Brzezinski, 1985). Thus, other considerations aside, the diatom phase of the bloom in waters with Si:N ~ 0.5 would be expected to run out of silicic acid, while roughly half of the entrained nitrate remains. Indeed, termination of the diatom phase of the North Atlantic spring bloom by silicic acid depletion has been documented (Leblanc et al., 2005; Sieracki et al., 1993) which favors use of the remaining nitrate by non-siliceous phytoplankton. This dual-phase character of the North Atlantic spring bloom is not absolute. Shallower winter mixing can favor dinoflagellates over diatoms during the initial stages of the bloom, suppressing overall diatom contribution (Henson et al., 2012).

While the depth of winter mixing dictates the inventory of silicic acid that can support a diatom bloom once the water column stratifies, physical factors that resupply silicic acid to surface waters control the continued diatom contribution following silicic acid depletion (Binetti et al., 2020). The North Atlantic is a highly dynamic physical environment that can resupply nutrients, including silicic acid, to Si-depleted surface waters, thus relieving Si-limitation and allowing further diatom growth. Diatom recovery from Si limitation can potentially be rapid as laboratory experiments show that diatoms recover from Si stress more readily than from limitation by other macronutrients such as nitrate, resuming growth within hours (De La Rocha & Passow, 2004). Sustained diatom productivity following initial silicic acid depletion has been demonstrated along upwelling fronts in the North Atlantic (Allen et al., 2005). However, other processes that entrain relatively nutrient-rich deep waters to the mixed layer, such as vertical mixing associated with storm activity, likely also promote continued diatom growth when surface silicic acid concentrations are low. The magnitude of the effect is set by the frequency and strength of the mixing events.

Silica production during spring in the North Atlantic can be significant. High rates of silicic acid uptake, 2–3 μmol Si L^{-1} d^{-1}, have been measured during the spring bloom (Brown et al., 2003), but these rates are often lower (Brown et al., 2003; Leblanc et al., 2005; Poulton et al., 2006), reflecting spatial and temporal variability within the bloom. Silica dissolution rates have not been measured in the North Atlantic, but are expected to be low during the diatom phase of the bloom (Brzezinski et al., 2003) such that the majority of silica production at this time would be expected to be supported by "new" silicic acid maximizing diatom export potential. Post-bloom, the reliance on silicic acid regenerated through the dissolution of frustules in surface waters tends to increase significantly (Brzezinski et al., 2003; Closset et al., 2014) and silica production rates along with new silica production and diatom export potential would generally be lower.

The dual-phase (diatom/non-diatom dominance) aspect of the North Atlantic spring bloom can strongly affect the biological pump. As inherently fast-growing, large, mineral- ballasted cells that can also form heavily silicified resting spores, diatoms follow relatively efficient export pathways through upper-ocean food webs including the sinking of individual cells, their consumption by larger mesozooplankton that produce large fast-sinking fecal pellets, and diatom incorporation into aggregates. These factors become modified when diatoms experience silicon limitation. While Si-limited diatoms have reduced frustule thickness (Martin-Jézéquel et al., 2000; Paasche, 1973) which impedes sinking, they also become more susceptible to grazing (Liu et al., 2016; Ryderheim et al., 2022). Si-limited diatoms also have reduced buoyancy following senescence or death (Krause et al., 2019) accelerating sinking rates, and they can have enhanced levels of polymeric cell coatings (Waite et al., 1995) that enhance adhesion facilitating aggregation and export (Billett et al., 1983; Thiel et al., 1989). The phytoplankton community that follows the diatom phase tends to be more diverse and comprised of smaller phytoflagellates and cyanobacteria (Lochte et al., 1993) that mostly lack mineral ballast with the notable exception of

coccolithophores. This succession is likely accompanied by additional changes in food-web dynamics that may drive differences in the efficiency of organic carbon export between the two phases of the bloom.

Studies of particle export document the importance of diatoms in the biological pump in the North Atlantic (Honjo & Manganini, 1993; Martin et al., 2011). Honjo and Manganini (1993) measured opal flux during the JGOFS North Atlantic bloom Experiment using sediment traps, reporting that opal flux at 2,000 m depth peaked a few weeks after silicic acid was depleted in surface waters. The peak in the opal flux coincided with a maximum in organic carbon export. Abundant intact single-celled diatom species were observed at depth, indicating rapid sinking rates. The sediment trap studies are corroborated by observations of large pulses of phytodetritus arriving at the sea-bed, including diatoms characteristic of the spring bloom (Billett et al., 1983; Thiel et al., 1989), emphasizing the importance of the aggregation export pathway to diatom blooms in the region. In contrast, Henson et al. (2012) found little correlation between diatom abundance in surface waters and organic carbon export at 3,000 m over an 11-year period at the Porcupine Abyssal Plain Sustained Observatory in the eastern North Atlantic, indicating both temporal and spatial variation in diatom contribution.

To further elucidate diatom-driven bloom dynamics in the North Atlantic, the present study sampled the North Atlantic spring bloom as part of the NASA EXport Processes in the Ocean from RemoTe Sensing (EXPORTS) program. The expedition began at the terminus of the diatom phase of the bloom, allowing examination of the processes that sustain diatom productivity following the depletion of silicic acid and the subsequent collapse and export of the main diatom bloom. We found that silica production and biogenic silica (bSi) export were still substantial following the terminus of the main diatom bloom, but that the levels observed were highly dependent on conditions that promoted the resupply of silicic acid to surface waters.

2. Methods

2.1. General Approach

The logistics and an analysis of the physical oceanographic context of the deployment of the EXPORTS program to the North Atlantic have been described in detail by Johnson et al. (2024). Briefly, the study was conducted in May 2021 within a retentive mesoscale eddy (designated as eddy A2) located approximately 170 km east of the site of the Porcupine Abyssal Plain Sustained Observatory (PAP-SO; Hartman et al., 2021). Data reported here were collected aboard two ships: the RRS *Discovery* and RRS *James Cook* that sampled the eddy from May 4 (year day, YD, 124) through May 30 (YD 150). Sampling aboard the *Cook* followed a Lagrangian float that tracked an isopycnal at around 90 m near the center of the eddy for the entire cruise. *Discovery* sampled a wider geographic area within an 85 km radius from the eddy center in survey mode (Figure 1, Figure S2 in Supporting Information S1). The eddy center was tracked throughout the cruise (Erickson et al., 2023) with sampling aboard *Discovery* adjusting to this moving frame of reference. Sampling aboard the *Cook* and the *Discovery* occurred in three approximately 8-day cycles, referred to as epochs (Siegel et al., 2021), organized around three sets of sediment trap deployments from the *Cook*. Export fluxes of particulate organic carbon (POC) and bSi export were also assessed on the *Discovery* using the ^{234}Th method tied to elemental ratios obtained from particles collected using in situ pumps (Clevenger et al., 2024).

2.2. Sampling and Analyses

Seawater samples for determining silicic acid ($Si(OH)_4$) and bSi concentrations were taken on both ships using common procedures. On the *Cook*, samples for both inorganic nutrients and particle composition were obtained on casts of a conventional CTD/rosette equipped with 12-L Niskin samplers. On the *Discovery*, samples for both parameters were collected using a similar conventional CTD/rosette system. Additional samples for these parameters and for rate processes were obtained on *Discovery* via casts of the ship's trace-metal-clean CTD/rosette system that was equipped with 10-L Go-Flo bottles to match procedures during the EXPORTS Northeast Pacific expedition to Ocean Station Papa (Brzezinski et al., 2022). All rosette systems were equipped with SeaBird 911 CTDs.

On each ship, seawater nutrient samples were collected from the upper 500 m and filtered through 0.2-μm polycarbonate filters into acid-cleaned plastic vials and immediately frozen at −20°C. On both ships, seawater samples for bSi concentration were obtained from the upper 175 m (*Discovery*) and the upper 125 m (*Cook*). They were processed by filtering 600–1,000 mL of seawater through 47-mm diameter, 0.6-μm pore-size polycarbonate

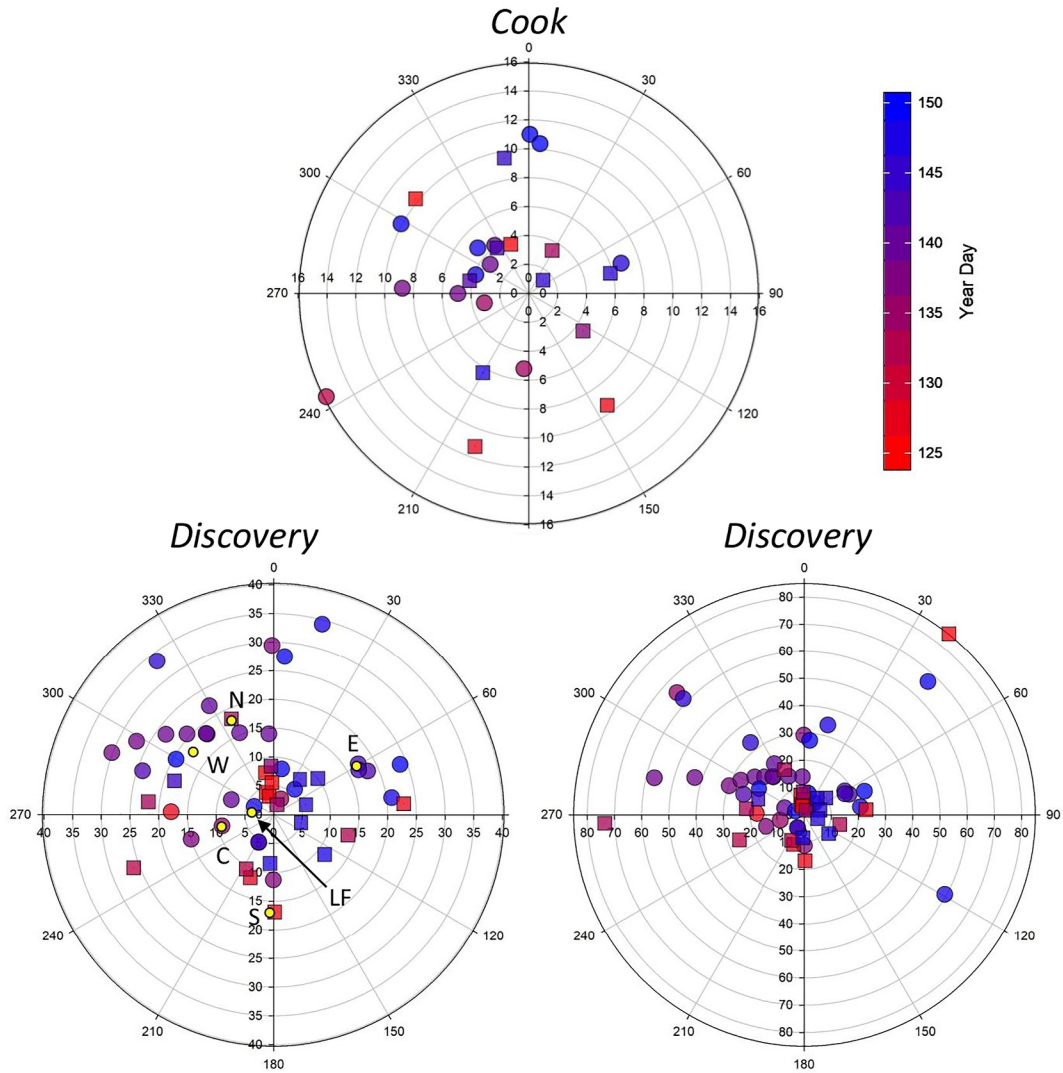

Figure 1. Station locations sampled aboard the *Discovery* and *Cook* plotted relative to the eddy center. Note differences in radial scaling among plots. Two plots are shown for *Discovery* scaled to different radial distances from the eddy center to better illustrate the extent of sampling and overlap with *Cook*. Circles denote stations where surface waters were of water type 1, warm/salty, and squares denote surface water type 2, cold/fresh, as defined in Johnson et al. (2024). Colors change from red to blue with time during the cruise as shown by the color bar. Labeled yellow symbols on the *Discovery* plot denote stations where size-fractionated silica production and size-fractionated bSi was measured (S: south, N: north, C: center, E: east, W: west, LF: Lagrangian float, see Text S1 in Supporting Information S1 for latitude and longitude).

filters. For all casts aboard *Discovery* that utilized the trace-metal rosette, seawater for bSi analysis was size-fractionated by sequential filtration of each sample through a 5.0-μm and then a 0.6-μm pore-size 47-mm polycarbonate filter. For all bSi samples, filters containing the particulate matter were folded, placed in a cryovial and dried at 60°C to prevent residual seawater from dissolving the opal.

At the end of the expedition, silicic acid samples from both the *Discovery* and the *Cook* were transported frozen on dry ice to the University of California Santa Barbara. Frozen silicic acid samples were heated at 50°C for 30–45 min to eliminate polymers of Si and then allowed to cool to room temperature before analysis (Becker et al., 2020). Nutrient samples from the trace-metal rosette were analyzed on a Lachet 8500 series 2 flow injection system. Samples from the conventional rosette systems were analyzed using a Seal Analytical continuous-flow Auto Analyzer 3. Both analytical systems had a detection limit of 0.2 μM silicic acid or 3%, whichever was larger. Automated nutrient analyses were calibrated against the SCOR-JAMESTEC lot CI certified reference material. For both analytical instruments, the measured silicic acid concentrations of the CRMs were within 2% of the

certified value. Samples for bSi from both ships were analyzed using the NaOH digestion method described by Krause et al. (2009) using manual colorimetry with a detection limit of 0.05 μmol Si L^{-1}.

Profiles of size-fractionated silica production rates were obtained on the *Discovery* using the radiotracer silicon-32 as sodium silicate (Brzezinski & Phillips, 1997). Six profiles, each sampling five depths spanning the 62% to the 1% light levels were obtained across the three epochs using the trace-metal-clean rosette system (Figure 1, Figure S1 in Supporting Information S1). All subsampling of Go-Flo samplers was conducted in the trace-metal-clean laboratory aboard *Discovery* and the subsamples were transferred within plastic bags to a radioisotope van for tracer addition. Seawater for rate measurements was subsampled into trace-metal-cleaned 300-mL polycarbonate bottles and then spiked with 280 Bq of Chelex—cleaned high-specific activity silicon-32 (15,567 Bq μg^{-1} Si). Each sample bottle was capped and the closure sealed with parafilm before being transferred to deck incubators that simulated the light levels at each sample collection depth using a combination of neutral density screening and blue plastic film. Incubators were cooled with flowing surface seawater. Following 24 hr of incubation, water samples were size-fractionated through 25-mm diameter 5.0-μm pore size filters followed by a 0.6-μm pore size polycarbonate filters paralleling the size-fractionation of bSi samples. Silicon-32 activity on the filters was measured using low-level beta detection, as in Krause et al. (2011).

The degree to which $Si(OH)_4$, NO_3^- or Fe limited rates of silica production was quantified at all six stations sampled using the trace-metal-clean rosette at the 40% light depth and at three stations at the 10% light depth. Si-amended (+Si) and N-amended (+N) treatments increased the concentration of each nutrient by 20 μM using Chelex-cleaned solutions of either sodium metasilicate or sodium nitrate. Fe additions (+Fe) targeted an increase of 1 nM Fe using ferric chloride. Combined treatments (+Si&Fe) and (+Si&N) used dual additions: 20 μM silicate & 1 nM Fe and 20 μM silicate & 20 μM nitrate, respectively. Samples of unamended seawater served as controls. Incubations were conducted for 24 hr. Treatment effects were assessed as the ratio of the silica production rate in the treatment relative to controls, which is termed the enhancement statistic (Enh). The experiment was replicated six times during the cruise, but treatments were not replicated within a single experiment. The silicate and nitrate stocks for the +Si treatment were analyzed for dissolved Fe. Based on those results, experimental additions of Si and N would raise ambient [dFe] by 0.05 nM. Immediately after amendments, Si production samples were spiked with silicon-32, incubated, and processed as described for silicon-32 rate profiles.

Cylindrical sediment-trap tubes (collection area 0.0113 m^2) were deployed at depths ranging from 75 to 500 m for periods of 2–5 days. Two types of trap platforms were used: a drifting, surface-tethered mooring (STT; epochs 1–3), and neutrally buoyant sediment traps (NBST; Estapa et al., 2020; epoch 3 only). Estapa et al. (2024) describe these deployments and the determination of POC fluxes. POC flux values are available at https://doi.org/10.5067/SeaBASS/EXPORTS/DATA001. Here we provide the details of bSi flux measurements. Each trap platform depth included two cylindrical tubes used for separate bSi flux determination. Tube preparation, trap deployment and trap recovery were as in Estapa et al. (2021). Final samples from each pair of tubes were combined and split into 8 equal fractions, three of which were processed for bSi analysis by filtering onto 25-mm diameter, 1-μm pore size polycarbonate membranes (Whatman Nuclepore), drying at 45°C in polycarbonate petri dishes, and storage of the dried filters at room temperature until analysis for bSi at the University of Maine. Then, half of each filter was analyzed for bSi content using the same procedures as described above for particles collected from seawater. Fluxes were computed by averaging the three splits and normalizing to the total collection area and elapsed time from deployment to lid closure. The bSi flux uncertainty was propagated from the split-to-split standard deviation and the median relative standard deviation for bSi fluxes was 5%.

3. Results

3.1. Environmental Context

The details of the environmental conditions encountered during the EXPORTS North Atlantic expedition have been published by Johnson et al. (2024). Briefly, data from gliders deployed prior to the cruise indicated that the initiation of the spring bloom, as indicated by the date of sustained heat flux zero crossing (Rumyantseva et al., 2019), occurred within eddy A2 about 15 days prior to the arrival of the ships. Thereafter, the mixed layer (ML) shoaled to 30 m and remained close to that depth for the week before the ships arrived. Chlorophyll *a* concentration within the eddy measured by the fluorometers aboard the gliders increased during this period and remained relatively high at the start of the cruise (Johnson et al., 2024).

Table 1
Intercalibration of Biogenic Silica and Silicic Acid Concentrations Between Ships

	Water type		Integrated bSi (mmol m^{-2})		Average $[Si(OH)_4]$ (μM)		Percent difference	
Year Day	*Cook*	*Discovery*	*Cook*	*Discovery*	*Cook*	*Discovery*	bSi	$Si(OH)_4$
127.7	Cold/fresh	Cold/fresh	81.6	83.9	0.10 ± 0.00	0.10 ± 0.0	2.8	0.0 ± 0.0
145.7	Warm/salty	Cold/fresh	57.1	47.1	1.10 ± 0.00	1.35 ± 0.07	17.5	22.7 ± 6.4
147.6	Warm/salty	Warm/salty	29.5	27.8	1.65 ± 0.07	1.75 ± 0.07	6.0	6.1 ± 6.0

Note. Uncertainty terms are standard deviations.

The core of the eddy below about 90–150 m had little horizontal exchange with adjacent waters for the duration of the cruise. Surface waters above this stable core were defined as Surface Core Waters (SCW, Johnson et al., 2024). Stations sampling SCW were almost always located within 15 km of the center of the eddy. Surface waters across the eddy, including SCW, showed small-scale variation in T/S properties and were classified as either warm/salty, water type 1 (WT1), or cold/fresh, WT2 (Figure 1).

A major driver of environmental variability was four separate storms that each entrained nutrients from below the mixed layer, mixed particles to depth and exchanged surface waters between the eddy and adjacent areas. Storms deepened mixed layers by 25–40 m (mixed-layer depth, MLD, assessment used a 0.05 kg^{-3} definition) and caused lateral exchange of SCW ranging from 20% to 75% with flushing times of 5.5–8.5 days (Johnson et al., 2024). One storm occurred at the end of epoch 1, two during epoch 2, and one during epoch 3.

3.2. Intercalibration Between Ships

On three occasions, *Cook* and *Discovery* both sampled SCW near the eddy center simultaneously when the two ships were within 0.3–0.5 km of each other to intercalibrate sensors and measurements. The ships were in the same surface water type based on T/S properties for two of the three intercalibrations (Table 1). To compare silicic acid concentrations, values from the upper 25 m (all within the mixed layer) were averaged for each ship on each occasion. For bSi concentrations, the values obtained from each ship were integrated into a common depth of 125 m using linear interpolation between sampling depths when necessary.

On the two occasions when the ships were in the same water type, the average 25 m silicic acid concentrations measured on the two ships were within 6% of each other (Table 1), whereas results differed by 23% when each ship sampled a different water type. Similarly, integrated bSi concentrations agreed to within 3%–6% when the ships were in the same water type, but differed by 18% when in different water types (Table 1). No corrections were applied to the data obtained from either ship.

3.3. Silicic Acid Concentration

Profiles of silicic acid concentration show surface waters with concentrations between 0.1 and 0.3 μM at the start of the cruise prior to the first storm (Figure 2, Figure S2 in Supporting Information S1). Concentrations increased with depth reaching 3–4 μM within the nutricline at about 50 m (Figure 2). Silicic acid concentration between the base of the mixed layer and 500 m showed less variation in the stable core of the eddy measured aboard *Cook* compared to stations sampled aboard *Discovery* that sampled across the eddy. When the vertical distribution of silicic acid concentration is examined relative to density (Figure S3 in Supporting Information S1) the high variability at depth in the data from *Discovery* remains indicating significant variability in silicic acid concentration in the upper mesopelagic away from the eddy center.

In contrast to the low surface silicic acid concentrations, nitrate was abundant in surface waters with concentrations between 4.8 and 5.2 μM in the upper 25 m across the eddy (Johnson et al., 2024; Meyer et al., 2023). Silicic acid concentration in surface waters increased to between 1 and 2 μM over time as the four storms entrained silicic acid into the surface waters (Figure 2; Johnson et al., 2024). This temporal trend is observed across the eddy (Figure 3a, Figure S2 in Supporting Information S1), both within the SCW near the eddy center and beyond, indicating that spatial variation was dominated by these temporal changes even outside the 15 km radius defining the SCW. Water type played a role in the observed variability. Average silicic acid concentrations

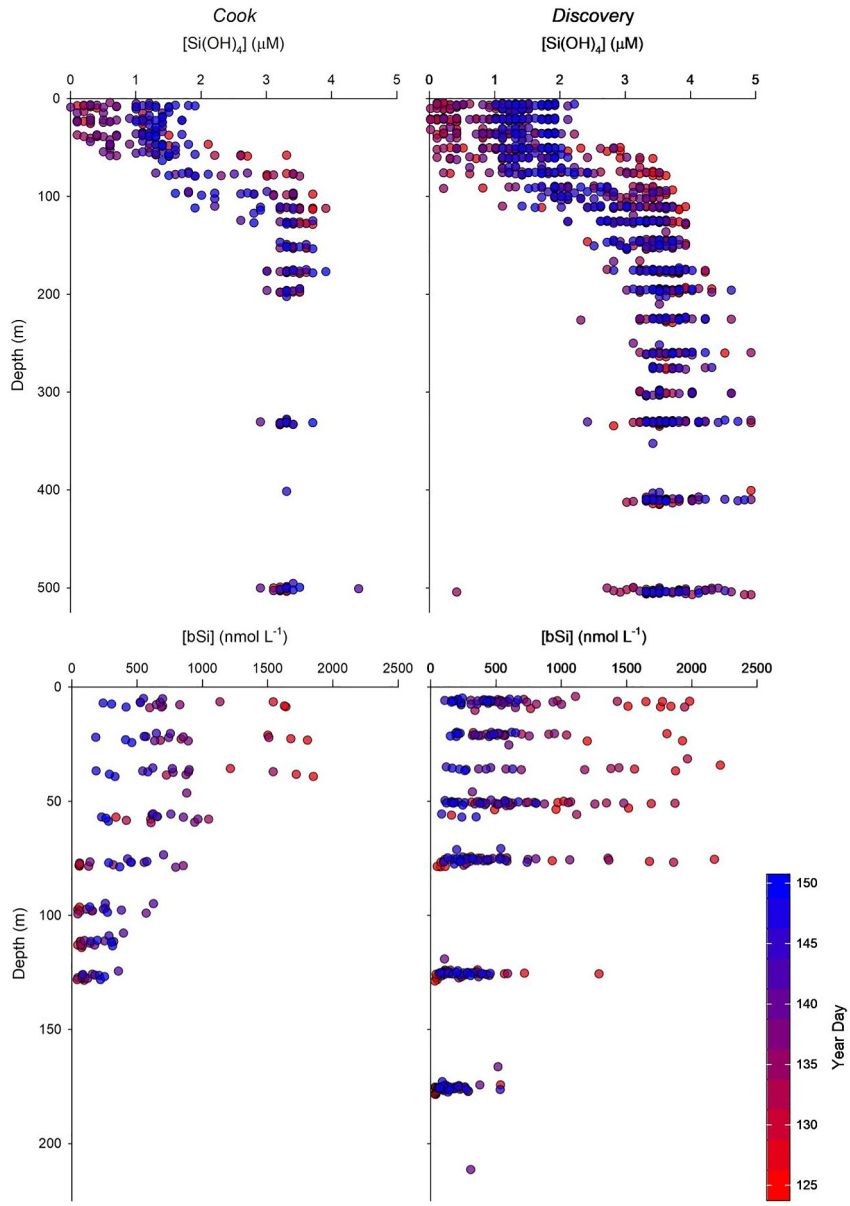

Figure 2. Depth profiles of silicic acid concentration (upper panels) and biogenic silica concentration (lower panels) from the *Cook* and *Discovery*. Colors reflect the date of sampling and transition from red to blue over time as indicated by the color bar.

in WT1 (warm/salty, 1.20 ± 0.09 μM) were statistically higher than in WT2 (cold/fresh, 0.77 ± 0.10 μM) (t-two tailed *t*-test, $p = 0.005$, d.f. = 65). Profiles of silicic acid and nitrate concentrations associated with casts of the trace-metal rosette were representative of the range of concentrations seen in the larger data set (Figure 4a).

3.4. Biogenic Silica Concentration

Biogenic silica concentration showed a pattern opposite to that of silicic acid in that bSi concentrations in the upper water column declined over time (Figure 2, Figure S2 in Supporting Information S1). The values were highest at the beginning of the cruise with values between 1.00 and 2.25 μmol L^{-1} declining to <0.1 μmol L^{-1}. As the method used to digest the bSi also dissolves and average of 15% of the lithogenic silica (LSi) present in the sample (Ragueneau & Tréguer, 1994) these values overestimate the actual bSi concentration. LSi was not routinely measured; however, their approximate influence on bSi measured on suspended particles and those in

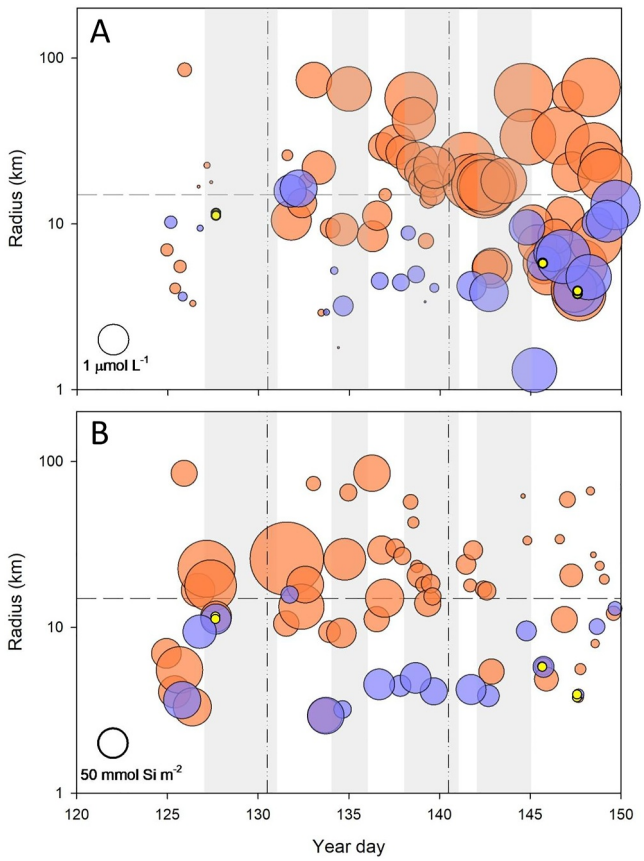

Figure 3. (a) Bubble plots of the average silicic acid concentration in the upper 25 m from *Cook* (purple) and *Discovery* (orange) as a function of the radial distance from the eddy center. (b) As in (a) except for integrated biogenic silica concentration in the upper 125 m. Values are proportional to bubble diameter. Bright yellow dots highlight stations where intercalibrations between the two ships were performed. Stations below the horizontal dashed line at 15 km radius are located in surface core waters. Vertical gray bars indicate time periods associated with storms and vertical lines define boundaries between epochs, as defined by Johnson et al. (2024).

traps can be estimated from LSi measurements from marine snow catchers in the upper 500 m (Romanelli et al., 2024). Assuming a 15% LSi contribution to the bSi digests yields an average LSi contribution of 8% ± 3% (std err., $n = 11$) to the measured concentrations of suspended bSi and 11 ± 5% (std. err., $n = 11$) for sinking bSi.

The pattern of declining bSi over time held across the eddy (Figure 3b, Figure S2 in Supporting Information S1) such that temporal changes in bSi dominated over spatial trends as seen for silicic acid concentration. Like silicic acid concentration, water type also contributed to variation in bSi concentration although the pattern was the reverse for bSi. Whereas the highest silicic acid concentrations were observed in WT1, the highest bSi concentrations occurred in WT2. Integrated bSi concentrations in the upper 125 m averaged 60.9 ± 5.2 mmol Si m^{-2} in WT1 and 101.4 ± 9.5 mmol Si m^{-2} in WT2, which is a statistically significant difference (two-tailed *t*-test, $p = 0.00002$, d. f. = 53). As was the case for silicic acid, the range of bSi concentrations from trace-metal rosette casts captured the range seen in the larger data set from both ships (Figure 4b).

Size-fractionated bSi concentration measured in the euphotic zone showed a strong dominance of the >5 µm fraction (hereafter referred to as the large size fraction) across the entire cruise (Figure 5a). On average 91.8% ± 0.7% (std. err., $n = 6$) of the bSi was in the large size fraction. As in the larger data set of total bSi concentration collected using the conventional CTD (Figure 2), bSi concentrations in the large size fraction collected using the trace-metal rosette declined over time, whereas changes in the concentration in the 0.6–5.0 µm fraction (hereafter referred to as the small size fraction) were less dramatic with concentrations remaining low and relatively constant (Figure 5a).

3.5. Silica Production

As was the case for bSi, silica production rates were dominated by the large size fraction (Figure 5b). Integrated rates were fairly constant in the large size fraction with the exception of one high value following the first storm, and a slight decline near the end of the cruise. Rates in the small fraction were initially very low but then rose somewhat during the first half of the cruise and remained elevated at modest levels (Figure 5b). In contrast, specific rates of silica production (V_b) increased by an order of magnitude in both size fractions over time, and they were still increasing at the end of the cruise (Figure 5c). At the beginning of the cruise, both size fractions exhibited similar V_b, but by YD 134 rates in the small size fraction exceeded those in the large size fraction and remained higher until the end of the cruise.

Comparison of integrated silica production rates to the integrated concentrations of bSi and silicic acid reveal dramatic changes in the implied turnover times for siliceous biomass and silicic acid. Turnover times for the large and small size fractions of bSi were initially 25 and 35 days, respectively, but through time both declined to values between 10 and 20 days after the first storm and to <10 days by the end of the cruise (Figure 5d). Silicic acid showed the opposite pattern with a turnover of <5 days at the start of the cruise that rose to near 40 days by YD 134 and remained near that level for the rest of the cruise (Figure 5d).

Although silica dissolution rates were not measured directly during the cruise, the extent of silica dissolution can be assessed as a cruise average for the mixed layer using estimates of silicic acid entrainment by storm mixing and mixed-layer integrated silica production rates. The change in dissolved silicic acid concentration (ΔDSi) over the cruise is related to the cumulative dissolution occurring in the mixed layer (D), cumulative entrainment of silicic acid across the four storms (E) and the cumulative loss to silicic acid uptake (ρ) as:

$$\Delta DSi = (D + E) - \rho \quad (1)$$

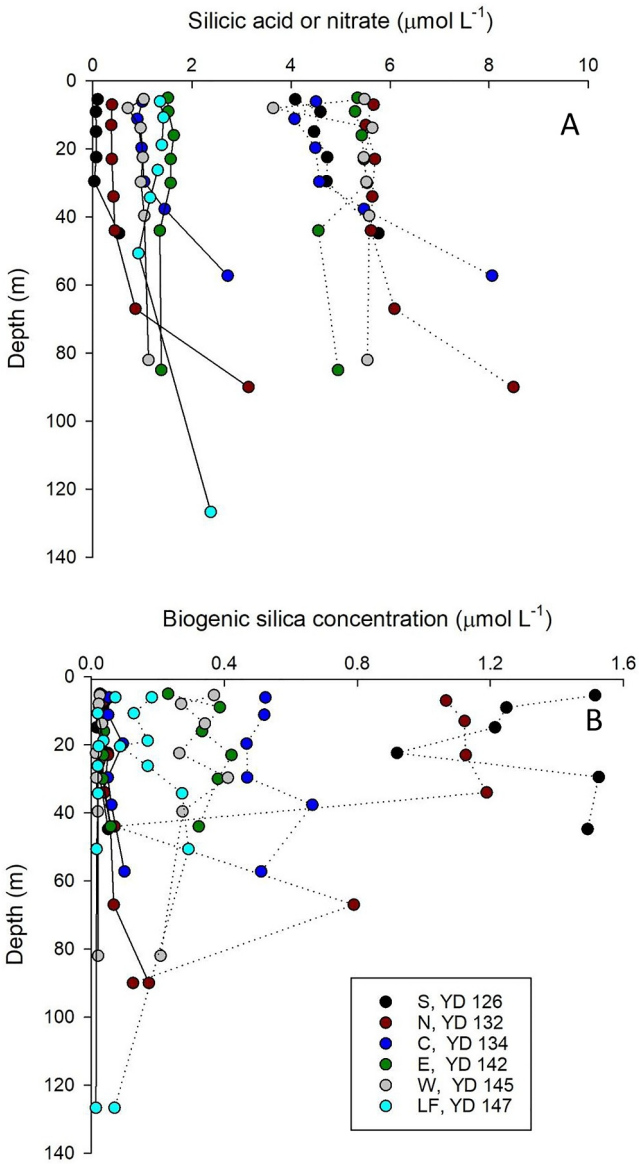

Figure 4. (a) Profiles of silicic acid (solid lines) and nitrate concentration (dashed lines) for stations sampled with the trace-metal rosette aboard *Discovery* with station designation (S: south, N: north, C: center, E: east, W: west, LF: Lagrangian float) and sampling date (Year Day, YD) as color-coded in the legend. Station locations are shown in Figure 1 using station designations. (b) Size-fractionated biogenic silica concentration from casts of the trace-metal rosette. Symbols as in (a). Profiles for the biogenic silica in small and large size fractions from a given station share a common symbol color with profiles for the large fraction having a dotted line and those for the small size fraction having a solid line.

Rearranging

$$D = (\rho + \Delta DSi) - E \quad (2)$$

where all variables have units of μM. Entrainment values for silicic acid have been estimated for each storm by Johnson et al. (2024) following procedures outlined in Text S5 of the Supporting Information S1. Combining those with the values of ρ and ΔDSi from the data reported here leads to an increase in DSi from dissolution of 1.55 ± 0.56 μM compared to a cumulative loss to production of 2.27 ± 0.05 μM bSi for a cruise average dissolution to production ratio of 0.68 ± 0.25 (Table 2).

3.6. Silicic Acid Limitation

The nutrient addition experiments provide strong evidence of silicic acid limitation. The addition of 20 μM silicic acid consistently increased silica production over ambient rates in the large size fraction at both the 40% and the 10% light depths (Figure 6). This response also consistently occurred in the small size fraction with the exception of the experiment on YD 134 when Si addition appeared to lower uptake rates in the experiment conducted at the 40% light depth. The stimulation of uptake by silicic acid was very strong, being over an order of magnitude in many cases. This is a clear indication of severe Si limitation of silica production. Stimulation by the silicic acid treatment was strong over the entire cruise (Figure 6); however, the extent of stimulation waned somewhat by the end of the cruise as ambient silicic acid concentrations in surface waters increased in response to storms.

Additions of nitrate and iron both failed to stimulate silica production (Figure 7) with median values indistinguishable from unity. In contrast, silica production rates were stimulated by silicic acid alone or when silicic acid was added in combination with nitrate or iron. The lack of response when nitrate and iron were added alone indicates that the observed stimulation in the +Si&Fe and in the +Si&N treatments was likely due to solely to the influence of the added silicic acid.

3.7. Sediment Trap Fluxes

To enable comparison of sediment trap bSi fluxes to silicon dynamics in surface waters, we focus on opal fluxes from the shallowest trap deployed 10–20 m below the mixed layer (Figure 8). The operational limits on deployment and recovery of traps during storms resulted in collection periods that spanned storm-driven changes in the mixed layer depth (Figure 8). As a result, NBSTs were unable to stabilize at the targeted 75 m depth during epochs 1 and 2, and during epoch 3, the uppermost STT trap (95 m) was within the mixed layer. However, useable samples were collected by STTs at 75 m during epochs 1 and 2, and an NBST at 109 m during epoch 3. All traps remained within 15 km of the eddy center within eddy core waters. The sinking bSi flux increased throughout the cruise, gradually from epoch 1 to epoch 2 and then more rapidly from epoch 2 to epoch 3 (Table 3). The bSi:POC mole ratio in exported particles more than doubled from epoch 1 to epoch 2 and then stabilized from epoch 2 to epoch 3 (Table 3).

4. Discussion

The time course of stratification and chlorophyll *a* response from gliders prior to the cruise combined with the relatively high bSi and extremely low silicic acid concentrations initially encountered aboard the ships indicated

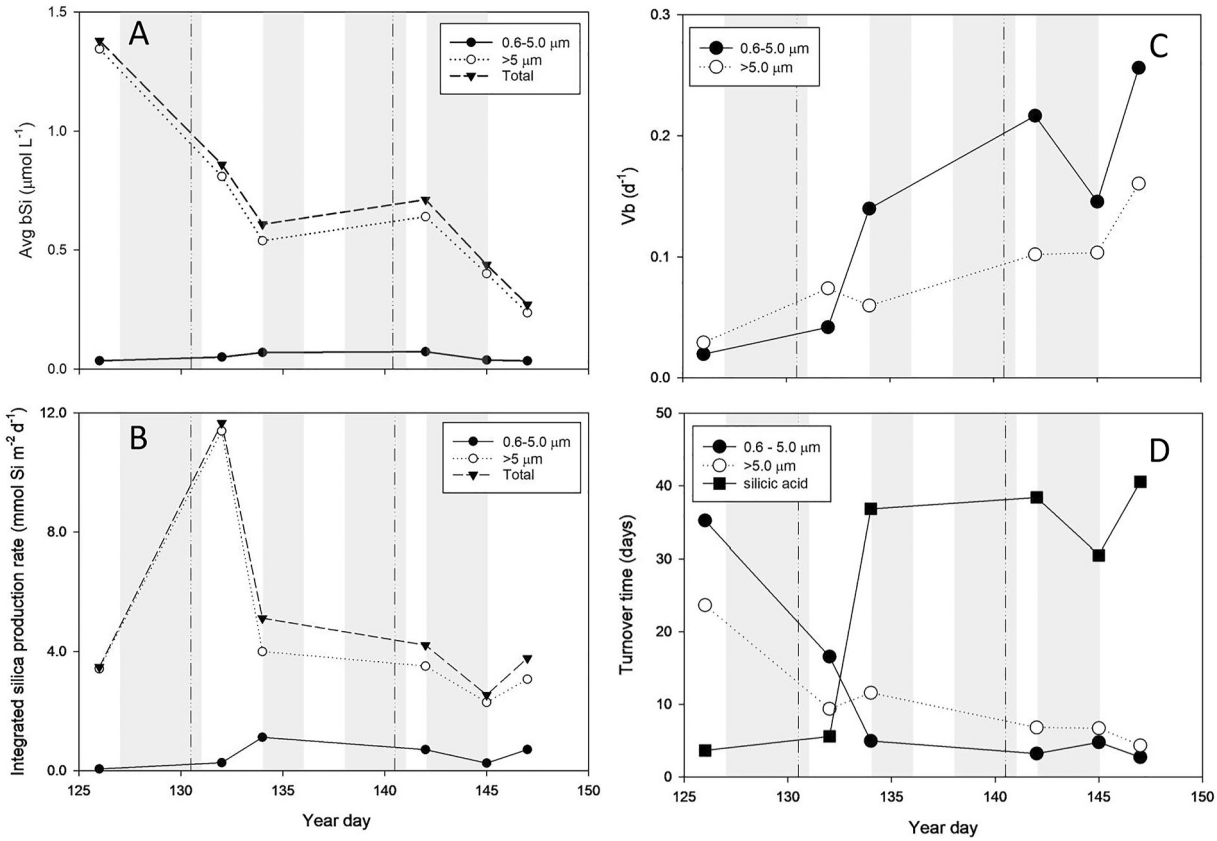

Figure 5. Time courses of properties in the euphotic zone: (a) integrated depth-normalized biogenic silica concentrations for size-fractionated bSi, (b) size-fractionated integrated silica production rates, (c) the average specific rate of silica production (V_b) in the large and small size fractions and (d) the turnover times of silicic acid and the two biogenic silica size fractions. Vertical gray bars indicate time periods associated with storms and vertical lines define boundaries between epochs, as defined by Johnson et al. (2024).

that a diatom bloom had occurred prior to the cruise that ended due to silicic acid depletion. Below, we place our findings during this post-bloom period in the context of past studies of Si cycling in the area. Then, we infer additional details of conditions prior to the arrival of the ships to gain a better perspective on conditions during the cruise. Finally, we relate diatom biomass and production dynamics in surface waters to measured rates of bSi and organic carbon export to assess how diatoms contributed to primary production and organic-carbon export following the collapse of the main diatom bloom.

4.1. Regional Context

Prior studies of silica cycling in the northeastern region of the North Atlantic are consistent with EXPORTS cruise having initially sampled the end of a diatom bloom (Table 4). The silicic acid concentrations encountered during EXPORTS are among the lowest reported though observations <2 µM appear typical. Integrated bSi concentrations and integrated silica production rates are both highly variable across and within studies, with values from EXPORTS being in the low to intermediate range compared to other investigations.

Table 2
Balance Between the Change in Silicic Acid Concentration (ΔDSi), Cumulative Silicic Acid Uptake (ρ), Cumulative Silicic Acid Entrainment (E), Cumulative Silica Dissolution (D), and the Silica Dissolution: Silica Production Ratio (D:P) in the Mixed Layer

ΔDSi (µM)	Cumulative Si uptake (µM)	Cumulative Si entrainment (µM)	Cumulative silica dissolution (µM)	D:P
1.21 ± 0.24	2.27 ± 0.05	1.93 ± 0.50	1.55 ± 0.56	0.68 ± 0.25

Note. Values are means ± one standard deviation.

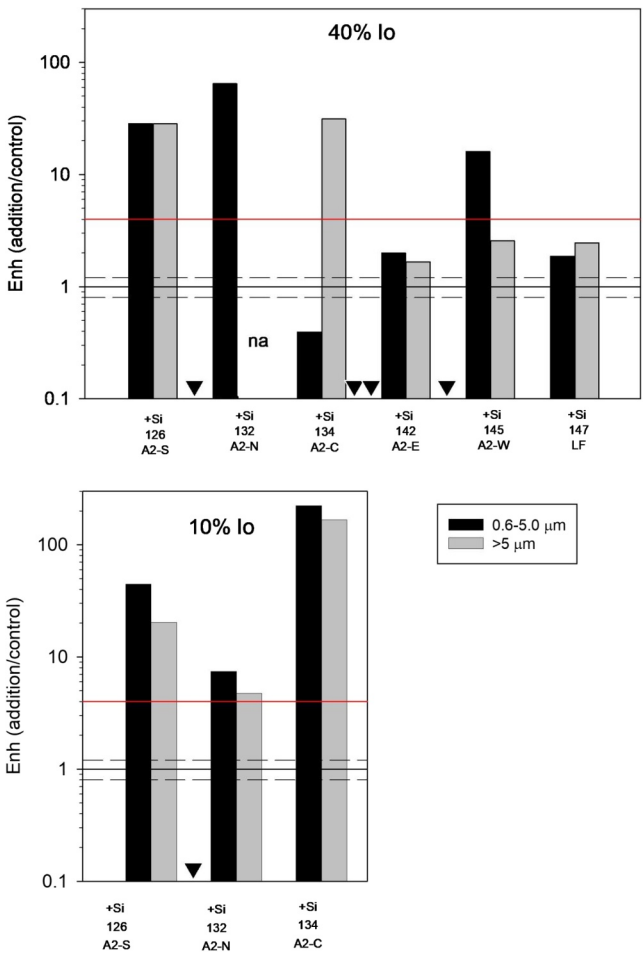

Figure 6. The enhancement statistic (Enh) for silicic acid uptake by the large and small size fractions at the 40% and 10% light depths. The horizontal solid line at Enh = 1 represents no effect of added silicic acid. The horizontal dashed lines represent the analytical uncertainty in the Enh estimates relative to a mean of 1, such that values need to be outside the range bounded by these lines to be considered different than unity. The horizontal red line at Enh = 4 is the threshold above which the growth rate is likely limited by the ambient silicic acid concentration. Inverted triangles indicate when storms occurred. Labels on the abscissa refer to the Si addition (+Si), the year day of the measurement with the designation A2 referring the eddy designation followed by the compass coordinate relative to eddy center as in Figure 1.

Prior studies have documented the termination of the North Atlantic spring diatom bloom through silicic acid depletion (Sieracki et al., 1993) and significant limitation of Si uptake during spring has been experimentally demonstrated (Leblanc et al., 2005). Leblanc et al. (2005) reported measurements of the ambient average V_b as a fraction of the maximum uptake rate, the inverse of which equates to the enhancement statistic (Enh) reported here. Their Enh values averaged 3.3 ± 2.2 ($1\sigma_{SD}$, $n = 11$, range 1.5–9.1) indicating consistent Si limitation of Si uptake (all values of Enh > 1) that ranged from modest to sufficiently severe to imply Si limitation of diatom growth rate (Enh > 4, see below). The severity of Si limitation during EXPORTS was significantly higher than that measured by Leblanc et al. (2005), especially early in the cruise period, reflecting the lower silicic acid concentrations encountered on EXPORTS, 0.1–0.3 µM prior to the first storm, versus the 1.0–2.5 µM values encountered by Leblanc et al. (2005).

4.2. The Initial Pre-Cruise Diatom Bloom

Insights into the magnitude and fate of the initial diatom bloom that occurred before the ships arrived can be assessed indirectly by comparing initial nutrient concentrations in the mixed layer at the beginning of the cruise to nutrient ratios in the subsurface waters that would be brought to the surface during winter mixing. That analysis assumes that during the bloom diatoms consume silicic acid and nitrate in a 1:1 ratio (Brzezinski, 1985), and it utilizes the nutrient measurements to diagnose a ratio of silicic acid to nitrate of 0.5 in the mesopelagic (see Text S4 in Supporting Information S1). The result is the following equation that quantifies the amount of silicic acid and nitrate utilized during the initial diatom bloom:

$$N_U = Si_U = (N_R - 2Si_R) \quad (3)$$

where N_U and Si_U are the amount of nitrate and silicic acid consumed (used) during the initial bloom, N_R and Si_R are the "residual" nitrate and silicic acid concentrations, respectively, that were measured at the beginning of the cruise. All variables have units of micromolar (µM).

The solution to Equation 3 indicates that the pre-cruise bloom consumed 4.6 µM each of nitrate and silicic acid with pre-bloom initial nitrate and silicic acid concentrations of 9.4 and 4.7 µM, respectively. Assuming that nutrient consumption occurred evenly over the euphotic zone, we estimate that total integrated silica production before the cruise was 3.1 times higher than that occurring during EXPORTS. The pre-cruise bloom occurred within a euphotic zone (1% light depth) that averaged 45 ± 5 m (s.d., $n = 35$, Johnson et al., 2024). Uniform consumption of 4.6 µM silicic acid over 45 m yields a total integrated silica production rate of 207 mmol Si m^{-2} compared to a total silica production rate of 67 mmol Si m^{-2} over the entire cruise (cruise average $\int \rho \times 26$ days).

The majority of bSi produced during the pre-cruise bloom appears to have been exported out of the surface waters before sampling began. During epoch 1 prior to the first storm, 1.3 ± 0.6 µM ($n = 11$) of the bSi produced during the pre-cruise bloom was still suspended in the surface waters. This implies that 3.3 µM silicon ([pre-bloom Si $(OH)_4$, 4.7] − [initial cruise bSi, 1.3] − [initial cruise $Si(OH)_4$, 0.1]) was no longer present as bSi or as $Si(OH)_4$ in surface waters. This implies that 72% (lost bSi, 3.3) ÷ (lost bSi, 3.3 + remaining bSi, 1.3) of the bSi produced during the initial bloom had already been exported prior to the cruise.

In summary, considering the production and export dynamics diagnosed above for the pre-cruise bloom, the diatom assemblage at the start of the cruise was a severely Si-limited remnant of a quite large and productive earlier bloom with the majority of bSi produced during the original bloom having already been exported.

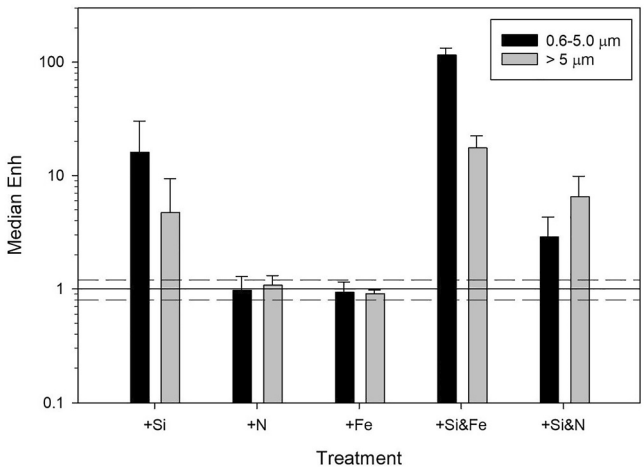

Figure 7. The median value of Enh for silicic acid uptake observed when samples were augmented with silicic acid alone (+Si), nitrate alone (+N), iron alone (+Fe) or with a combination of silicic acid and iron (+Si&Fe) or silicic acid and nitrate (+Si&N). Errors are median absolute deviations. Horizontal line at Enh = 1 represents no change with treatments. Horizontal dashed lines represent the analytical uncertainty and thus all values within those bounds are not considered different from unity.

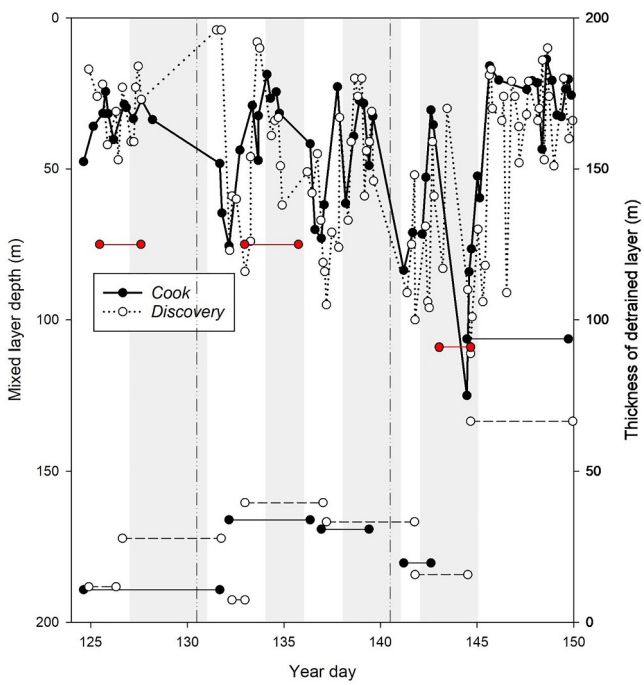

Figure 8. Changes in mixed-layer depth over time for CTD casts on *Discovery* (dotted lines) and *Cook* (solid lines) along with the depth and duration of sediment trap deployments (horizontal red lines). Dashed and solid black horizontal line segments are the thickness of the layer isolated below the mixed layer upon re-stratification following storm-induced mixing using data from *Discovery* and *Cook*, respectively. Vertical gray bars indicate time periods associated with storms and vertical lines define boundaries between epochs, as defined by Johnson et al. (2024).

4.3. Post-Diatom-Bloom Dynamics

The nutrient addition experiments revealed significant Si limitation of silicic acid uptake over the entire cruise with little influence of added nitrate or iron. The lack of effect of added nitrate was not surprising. The high ambient nitrate concentrations (~5 µM) would not be considered limiting to most diatoms. The lack of an effect of added Fe is less conclusive as short-term experiments (≤24 hr) often fail to detect an effect of added Fe on macronutrient uptake in low Fe waters. For example, Brzezinski et al. (2022) found no effect of 1 nM Fe additions on silicic acid uptake over 24 hr at Ocean Station Papa in the Northeast Pacific despite clear evidence for Fe limitation of diatoms during longer-term experiments (days) on the same cruise.

The Si limitation of Si uptake before the first storm was so severe that low silicic acid concentrations were likely limiting diatom growth rates. Diatoms compensate for the limitation of silicic acid uptake by thinning their frustules in proportion to the reduction in the rate of uptake, which leaves the time required to construct the frustule (i.e., the doubling time) largely unchanged. Diatoms have a finite, but significant, capacity to thin their frustules to where Si-limited cells can reduce the Si content by a factor of 2–4 after which the physiological capacity to thin the frustule cells is exceeded and the cells become growth-rate limited by Si. Thus, an Enh of 4 is a semi-conservative threshold above which the diatom growth rate is likely to be limited by Si. Figure 6 shows that up to and including YD 134, Enh values in both size fractions were almost always greater than 4 at both the 40% and 10% light depths, implying growth limitation of diatoms by Si. By YD 142 and thereafter, Enh values were most often >1, but <4 implying relief from growth rate limitation, while uptake limitation persisted.

Trends during the cruise point to continued silica production mediated in part by entrainment of high-nutrient subsurface waters during storms. Silicic acid concentrations in surface waters were initially 0.1 µM. Concentrations began to rise after the first storm, which exchanged 75% of SCW with adjacent waters (Johnson et al., 2024) and the rise continued with successive storms (Figure 3a, Figure S2 in Supporting Information S1). Increases in silicic acid happened earlier outside the 15 km limit defining SCW, but were everywhere higher after the third storm. These changes in silicic acid concentration were mirrored by those of bSi, which decreased over time (Figure 3b, Figure S2 in Supporting Information S1). Biogenic silica concentrations were over 1.0 µmol Si L^{-1} at the beginning of the cruise. Remanent high bSi values were occasionally observed after the first storm (Figure 3b, Figure S2 in Supporting Information S1), but after the second storm, values were consistently lower with continued decline following the third and fourth storms.

Despite the changes in dissolved and particulate Si, the measured rates of integrated silica production were fairly constant in the large size fraction (ignoring the one exceptionally high value on YD 132) and rose modestly in the small fraction after the first storm (Figure 5b). The consistency in volumetric rates runs counter to the large temporal increase in V_b that occurred as silicic acid concentrations rose (Figure 5c). The lack of an increase in integrated silica production against significantly increased V_b is consistent with the decline in bSi stocks over time as silica production is the mathematical product of bSi and V_b. The episodic pulsed resupply of silicic acid by the four storms helped relieve Si limitation to where the turnover time of bSi declined by over 3-fold in each size fraction, while the turnover time of the nutrient

Table 3
Sediment Trap bSi Flux and bSi:POC Ratio at the Uppermost Sampling Depth by Epoch

	Epoch 1	Epoch 2	Epoch 3
Depth (m)	75	75	109
bSi flux (mmol Si m^{-2} d^{-1})	1.15 ± 0.07	2.51 ± 0.21	5.80 ± 0.45
bSi:POC	0.10 ± 0.02	0.28 ± 0.05	0.26 ± 0.04

Note. Values are means ± one standard deviation.

rose by nearly an order of magnitude from a few days to over a month (Figure 5d).

The observation that the large size fraction dominated both total bSi concentration and total silica production is not surprising as large diatoms are known to dominate the early phase of the North Atlantic spring bloom. What was unexpected was that V_b in the small size fraction became consistently higher than in the large size fraction during epochs 2 & 3 (Figure 5c). A similar pattern was observed during the EXPORTS northeast Pacific cruise to Ocean Station Papa that employed the same size-fractionation techniques used here (Brzezinski et al., 2022). For the northeast Pacific study, Brzezinski et al. (2022) concluded that Si uptake in the small size fraction was most likely due to the presence of small diatoms rather than cyanobacteria like *Synechococcus* that are known to contain significant amounts of Si (Baines et al., 2012; Ohnemus et al., 2016). For the North Atlantic, integrated abundances of *Synechococcus* in the euphotic zone (1% light depth) averaged $1.4 \times 10^{12} \pm 1.5 \times 10^{12}$ (1 σ_{SD}, $n = 16$) cells m^{-2} (Graff JR, personal communication). *Synechococcus* abundance was converted to bSi content following Brzezinski et al. (2022) using a cellular Si content of 46 amole Si $cell^{-1}$ (Ohnemus et al., 2016) yielding an estimated integrated bSi concentration of 0.06 ± 0.07 mmol Si m^{-2}. That value is only 2.6% ± 3.0% (1 σ_{SD}, uncertainty term is the propagated error) of the average integrated bSi concentration in the small size fraction and thus so low that *Synechococcus* are not likely to be responsible for the observed Si uptake in this size class. Small diatoms of the genera *Minidiscus*, *Minutocelllus*, and *Nanoneis* are known to occur in the North Atlantic, with *Minidiscus* found to bloom under low silicic acid conditions, as observed here (Leblanc et al., 2018; Savidge et al., 1995). Thus, similar to the northeast Pacific, such small diatom taxa may be responsible for the biomass and activity in the small size fraction observed here in the North Atlantic.

The role of silicic acid as a limiting nutrient evolves over the course of the North Atlantic spring bloom. The depth of winter mixing sets the initial silicic acid inventory that is present in surface waters upon bloom initiation. Given the low silicic acid to nitrate ratios in subsurface waters, that concentration sets the magnitude of the yield of diatom biomass during the initial bloom. Dynamics after silicic acid depletion shift with continued silica production and additional diatom biomass yield controlled using physical processes that entrain silicic acid into surface waters. Thus, the relative magnitude of net silica production during the initial bloom and afterward are both set by the extent of physical mixing, which both determines the inventory of silicic acid for the initial bloom and the extent of resupply afterward. In the case of this post-bloom study, a series of four storms repeatedly entrained silicic acid into the surface waters leading to an increase in silicic acid concentrations from 0.1 to over 2 μM over 26 days. Entrainment during the storms partially relieved Si limitation, as indicated by declining Enh and rising V_b. Total silica production summed over the cruise was 32% of that estimated for the initial bloom, indicating substantial continued silica production under conditions where silicic acid was persistently limiting the rate of silica production. That value may be atypical as the number of high wind stress days encountered during May on the EXPORTS cruise was three times the 10-year average for that month at this location (Johnson

Table 4
Measures of Silicic Acid Concentration, Integrated Biogenic Silica Concentration and Integrated Silica Production in the Euphotic Zone of the North Atlantic During Spring and Summer

Location	Lat, °N	Season	DSi (μM) Range	∫bSi (mmol m^{-2}) Range	∫ρ (mmol Si m^{-2} d^{-1}) Mean	∫ρ (mmol Si m^{-2} d^{-1}) Range	Reference
Porcupine Abyssal Plain	48.8	Summer	NA	NA	0.9	0.5–1.3	Ragueneau et al. (1997)
Northeast Atlantic	35.5–46.3	Spring	<2.0	2.90–4.6	0.4	0.2–0.9	Poulton et al. (2006)
Northeast Atlantic	40.0–43.5	Spring (March)	1.6–2.5	4.0–8.0	0.9	0.6–1.5	Leblanc et al. (2005)
Northeast Atlantic	40.0–43.5	Spring (April)	1.0–1.5	9.0–61	4.3	0.7–11.2	Leblanc et al. (2005)
Northeast Atlantic	57.0–64.0	Spring	0.3–5.5	10.2–148	36	6–167	Brown et al. (2003)
Northeast Atlantic	49.0	Spring	0.1–2.1	2.7–65	2.6	1.2–5.8	This study

Note. Integrations are to the depth of the 1% light depth.

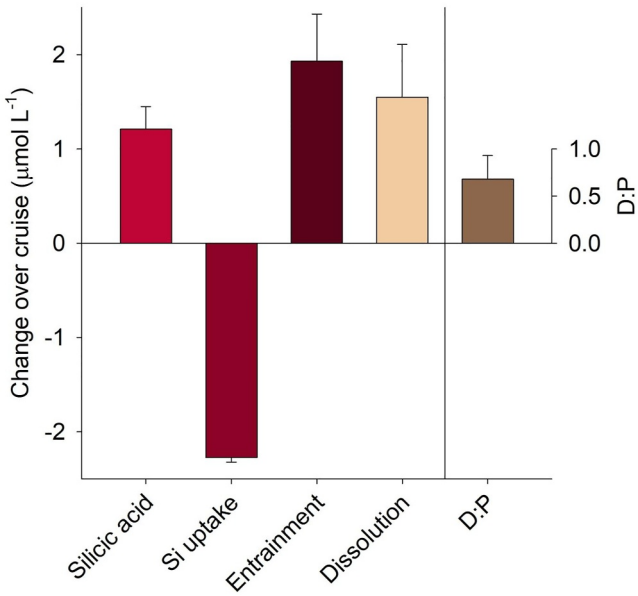

Figure 9. Cumulative net change in silicic acid concentration over the entire cruise compared to losses from Si uptake and gains from entrainment and dissolution together with the dissolution:production (D:P) ratio. Uncertainty bars represent standard deviations.

et al., 2024). However, other potentially more persistent mechanisms, such as upwelling along fronts, will also contribute to this process across the North Atlantic (Allen et al., 2005).

Silica dissolution also played a significant role in sustaining the observed silica production. Biogenic silica dissolution is the main source of regenerated silicic acid in surface waters and supports gross silica production, but at steady-state it cannot support net production. The balance of processes governing silica dynamics over the cruise are summarized in Figure 9 and Table 2. The net change in silicic acid concentration reflects losses due to uptake by diatoms opposed by resupply through silicic acid entrainment and frustule dissolution (Equation 1). Interestingly, the magnitude of the resupply from silica dissolution is 80% of that from physical entrainment, indicating nearly equal contributions from bSi dissolution and physical mixing in supporting silica production. The dissolution to production ratio (D:P) ratio of 0.68 is higher than the global average of 0.5 (Tréguer et al., 2021). D:P ratios transition from low values of about 30%–40% during blooms to values of 60%–90% or higher during post-bloom conditions (Brzezinski et al., 2003; Closset et al., 2014). Thus, it is expected that the estimated D:P during the post-diatom bloom period sampled here falls within the range of previous post-bloom estimates. Despite high losses due to dissolution, the level of new silica production (1 − D:P) is still 0.32, indicating significant export potential for diatoms.

4.4. Contribution of Siliceous Phytoplankton to New and Primary Production

The contribution of diatoms to the production of organic matter was partially driven by shifts in their abundance over time. The decline in bSi concentration over the cruise (Figure 3b, Figure S2 in Supporting Information S1) is consistent with an overall decline in chlorophyll *a* concentration and a shift in phytoplankton diagnostic pigment composition away from those contained in microplankton to pigments representative of smaller nanoplankton (Meyer et al., 2023). Moreover, Meyer et al. (2023) found that organisms containing fucoxanthin, often taken as indicative of diatoms, comprised 70%–80% of total chlorophyll *a* before the first storm. Fucoxanthin contribution then declined to between 30% and 50% for the rest of the cruise being largely replaced by 19'- hexanoyloxyfucoxanthin indicating a shift to haptophyte relative dominance. While concentrations of both bSi and pigments indicate a declining contribution from diatoms, these biomass indices also indicate that diatoms remained relatively abundant throughout the cruise.

Diatoms appeared to contribute significantly to new and primary production despite severe Si limitation. Diatom contribution to nitrate uptake and carbon fixation is often calculated using average diatom Si:N and Si:C ratios obtained from nutrient-replete culture studies (e.g., Brzezinski, 1985). However, under the Si-limiting conditions observed during this study, diatoms thin their frustules while maintaining near Redfield C:N ratios (De La Rocha & Passow, 2004), lowering the Si:N and Si:C mole ratios in Si-limited diatoms by 2- to 4-fold (Martin-Jézéquel et al., 2000). Si limitation ranged from severe to modest, so we adopted a 3-fold change in Si content when estimating the overall diatom contribution. Because profiles of silica production were made on a different ship than those of new and primary production, we averaged all integrated rates for a given property from each ship over the entire cruise before making comparisons. Utilizing the $^{15}NO_3$ uptake profiles (Meyer et al., 2023) and ^{14}C—primary production profiles (https://doi.org/10.5067/SeaBASS/EXPORTS/DATA001) that were both obtained aboard the *Cook*, this approach leads to an estimated contribution of diatoms to new and primary production of 88% ± 78% and 91% ± 63%, respectively, where uncertainty terms are the propagated standard deviations. The large uncertainty terms reflect the decline in each property over time, which caused the coefficient of variation about the mean for the cruise-averaged rates to be ~60% for both N and Si use and 27% for C productivity. The large uncertainty notwithstanding, the estimates imply a significant contribution of diatoms to new and primary production where, despite pervasive and persistent Si limitation, diatoms may have dominated both processes.

Table 5
Fractions of Euphotic Zone Silica Production and Integrated Biogenic Silica Exported From Surface Waters

Epoch	Depth of export (m)	bSi export (mmol Si m^{-2} d^{-1})		EZ ratio bSi-NPP[a] (%)		EZ ratio bSi-NCP[b] (%)		Export: $\int$bSi (% d^{-1}) *Discovery*		Export: $\int$bSi (% d^{-1}) *Cook*	
		Traps	^{234}Th	Traps	^{234}Th	Traps	^{234}Th	Traps	^{234}Th	Traps	^{234}Th
1	75	1.15 ± 0.07	3.6 ± 0.8	66 ± 17	207 ± 69	207 ± 53	647 ± 181	1.0 ± 0.4	3.2 ± 1.7	1.5 ± 0.4	4.5 ± 1.7
2	75	2.51 ± 0.21	3.2 ± 0.4	60 ± 33	76 ± 43	187 ± 104	238 ± 134	2.2 ± 1.0	2.8 ± 1.4	3.2 ± 0.8	4.0 ± 1.1
3	109	5.80 ± 0.45	5.9 ± 0.4	330 ± 82	336 ± 86	1,031 ± 256	1,050 ± 453	5.1 ± 2.2	5.2 ± 2.2	7.3 ± 2.0	7.4 ± 2.0

Note. Uncertainty terms are standard deviations. [a]Based on ^{32}Si silica production rates, which reflect net incorporation of DSi into bSi (Brzezinski et al., 2022). [b]Based on ^{32}Si silica production rates after accounting for losses due to silica dissolution in the euphotic zone (Brzezinski et al., 2022).

4.5. Relationship to Export

The EZ ratio (flux/production, Buesseler & Boyd, 2009) for bSi was calculated as follows (Table 5): Flux estimates are obtained from sediment traps and the ^{234}Th method (epoch averages, Clevenger et al., 2024). Two silica production estimates were used (bSi-NPP and bSi-NCP, Table 5). The first estimate comes from the silica production rates, bSi-NPP, measured using ^{32}Si. Those rates reflect the net rate of Si incorporation into particles after any efflux of dissolved Si out of the cells following its uptake, making these rates conceptually equivalent to net primary productivity (NPP) for organic carbon (Brzezinski et al., 2022), which is the parameter most often used to calculate EZ ratios for POC (Buesseler & Boyd, 2009). When silica production rates are adjusted for the losses of bSi due to silica dissolution (bSi-NCP), those rates become analogous to net community production (NCP) for organic carbon that accounts for respiratory losses of C within the entire upper ocean food web (Brzezinski et al., 2022). At steady state, bSi-NCP would be equivalent to the rate of export of bSi out of the euphotic zone.

The low, Si-limited rates of silica production meant that bSi export nearly equaled and sometimes exceeded the bSi-NPP rates. Exports often exceeded bSi-NCP rates by several fold (Table 5). Sustained bSi export at rates that exceed its rate of production likely relied on the relatively high initial standing stock of bSi in the euphotic zone. The fraction of integrated bSi that was exported was <5% d^{-1} during epochs 1 and 2 with the fraction increasing to 5%–7% d^{-1} during epoch 3 (Table 5). Biogenic silica export rates in excess of silica production are consistent with the decline in bSi stocks over the course of the cruise (Figures 3b and 5a).

Comparison of Si:C mole ratios in particles from the euphotic zone to those captured in sediment traps at 75–109 m reveals a strong temporal decoupling between bSi and POC export. Average Si:C mole ratios in the upper 25 m of the euphotic zone and those in sediment traps were both nearly equal at 0.10 during epoch 1 when the highest bSi concentrations were observed (Figure 10). By epoch 2, the ratios had diverged with declining Si:C in the euphotic zone and a large increase in sediment traps. The decline in the euphotic zone continued through epoch 3, while the high ratio in sediment traps was maintained. A similar trend has been observed in >5 μm particles collected by in situ pumps during the cruise (Clevenger et al., 2024). These differences in particle composition between surface waters and traps are affected by both physical and biogeochemical processes. The lateral displacement of surface waters by the storms (Johnson et al., 2024) could alter the surface particle assemblage as could changes in the relative rates of production and recycling of particulate Si and C.

There is little information about the particle composition of waters that were advected into the eddy by storms, which hampers the evaluation of the influence of that process on particle dynamics. However, the data do allow an assessment of the possible biogeochemical processes involved. Other considerations aside, the divergence in Si:C ratios between particles in the euphotic zone and those captured in traps points to a shift in the relative rate of recycling of bSi versus POC with time over the cruise. The equivalence of the two ratios during epoch 1 implies the congruent export of particles from surface waters with low, or proportional, losses of bSi and POC between the base of the euphotic zone and the sediment trap at 75 m. The subsequent divergence in Si:C between particles in traps and those in the euphotic zone implies that after epoch 1, POC export efficiency transitioned from being similar to that of bSi to being 5–10 times less efficient. This could arise if bSi was preferentially exported from the surface particle pool and/or if POC was lost preferentially during export. The preferential export of bSi is supported by observations of empty diatom frustules in marine snow catchers (Romanelli et al., 2024) and the

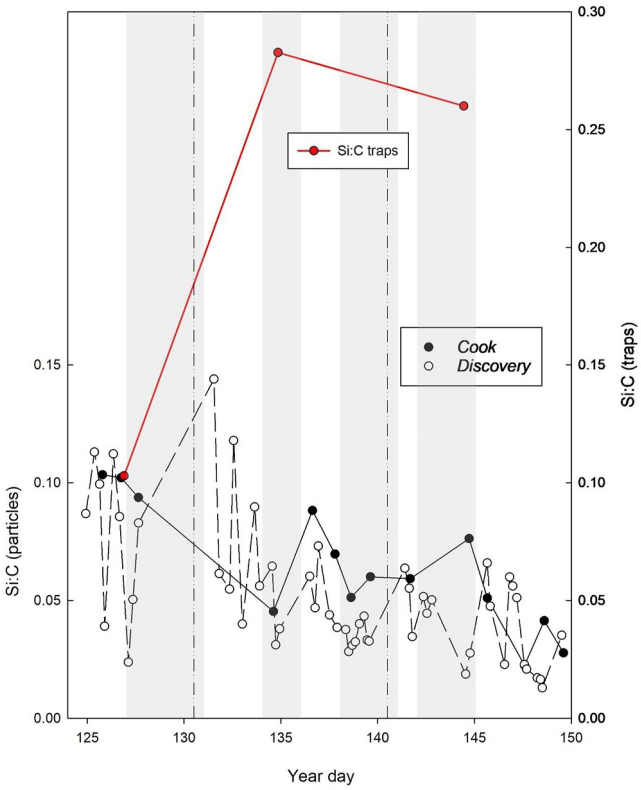

Figure 10. Change in the average silicon to carbon mole ratio (Si:C) within particles over time. Black and white circles represent data from the upper 25 m from *Cook and Discovery*, respectively. Red circles and lines are the Si:C ratios in particles from sediment traps. Vertical gray bars indicate time periods associated with storms and vertical lines define boundaries between epochs, as defined by Johnson et al. (2024).

increase in the fraction of integrated bSi that was exported over time (Table 5); however, the increase was modest and offset by the declining bSi stocks during the cruise. Flux profiles from ^{234}Th disequilibria support the possibility of differential remineralization of POC over bSi (Clevenger et al., 2024). During epoch 1, the flux profiles of POC and bSi essentially parallel each other in the upper 100 m, while during epochs 2 and 3, the export of POC attenuates and that of bSi increases between the mixed layer and 100 m (Clevenger et al., 2024).

When the contribution of diatoms to POC flux is calculated using the same Si:C conversion ratio used for estimating diatom new and primary production, the trap-based contribution ranges from 26% to 72% and the ^{234}Th-based contribution ranges from 84% to 110%. These estimates imply that diatoms dominate POC flux similar to their implied dominance of new and primary production. However, the conversion factor used reflects the elemental ratios of living Si-limited diatoms. Using that ratio for export implicitly assumes that all diatoms are exported as intact cells, which, though supported by some observations of phytodetritus at depth in this region (Billett et al., 1983; Thiel et al., 1989), is generally unrealistic as organic matter is often recycled faster than bSi. Clevenger et al. (2024) provide depth-resolved bSi and POC fluxes that show POC fluxes attenuate significantly between the mixed layer and 100 m during epochs 2 and 3, whereas they increase slightly in this depth zone during epoch 1. If we assume that diatom POC attenuates similarly to bulk POC, then diatoms account for between 40% (range 26%–52%) and 77% (range 49%–101%) of the POC flux averaged across epochs for estimates from traps and ^{234}Th, respectively.

4.6. Storm Effects on bSi Export

With four storms over 26 days, physical processes had a large impact on export dynamics during the cruise. That differs from the conditions prior to the cruise when the mixed layer remained at 30 m for over a week and a strong increase in chlorophyll *a* concentration indicated the development of the pre-cruise bloom in the relatively stable water column (Johnson et al., 2024). That prolonged period could have led to a scenario where the initial diatom bloom peaked with the ensuing Si limitation driving diatom aggregation and export as has been previously inferred for the North Atlantic spring diatom bloom (Sieracki et al., 1993). The lower biomass and increased turbulence during the cruise altered export dynamics relative to this canonical bloom-aggregation-export scenario. An analysis of large-particle size spectra shows that oscillations in mixed-layer turbulence caused by repeated storms drove both particle aggregation and disaggregation (Siegel et al., 2024). Data collected with marine snow catchers show that fast-sinking aggregates (diameter >0.1 mm) were relatively rare during most of the cruise, but that their volumetric concentration increased exponentially during the last days of the cruise in epoch 3 after the fourth storm and after the last sediment trap recovery (Romanelli et al., 2024). The aggregation event increased the calculated total POC flux at 95–125 m depth by a factor of 4 over that measured earlier in epoch 3 in traps (Romanelli et al., 2024). Analysis of 18S rDNA (V4 region) sequences from individually picked aggregate particles (Durkin et al., 2022) indicated that diatoms had the highest relative abundance compared to other phototrophic phytoplankton in these particles (mean = 56.3%, median = 55.7%, standard deviation = 23.9%, range = 5.2–96.0%, Durkin et al., 2022), suggesting that diatoms accounted for a sizable fraction of the phytoplankton component of exported organic matter in aggregates.

The influence of storms extended deeper than their effect on turbulence within the mixed layer through the action of the mixed-layer pump (Dall'Olmo et al., 2016; Gardner et al., 1995). Each storm deepened the mixed layer followed by stratification that re-established the mixed layer at a shallower depth (Figure 8). Given the higher concentration of particles in surface waters, mixed-layer deepening led to their detrainment, moving particles from the surface to deeper waters and diluting their concentration in the now deeper mixed layer. Re-stratification then isolated a portion of the detrained particles below the new shallow mixed layer. With no further mixing, these particles were thus "pumped" to depth and isolated away from surface turbulence, potentially fostering particle

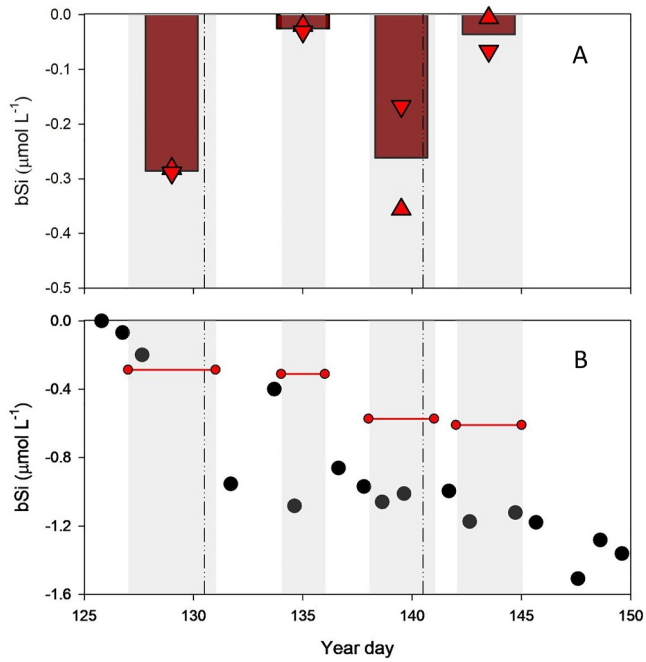

Figure 11. Change in bSi concentration within the mixed layer of surface core waters caused by entrainment of low bSi waters during storms: (a) Change in bSi (bars) due to entrainment for each storm event (shaded gray areas). The triangles are the flux from estimates of ΔbSi ÷ Δt and the upside-down triangles are the bulk estimate from changes in mixed-layer depth, with the bar graph being the average of the two (see Text S5a in Supporting Information S1). (b) Horizontal red lines represent the cumulative decrease in bSi concentration in the mixed layer due to entrainment (i.e., cumulative sum of colored bars in (a)). The circles are changes in the average mixed-layer bSi concentrations relative to the average bSi concentrations at the beginning of epoch 1. Vertical gray bars indicate time periods associated with storms and vertical lines define boundaries between epochs, as defined by Johnson et al. (2024).

sinking. As there were less than 5 days between storm events, particles oscillated between being within shallow mixed layers and being isolated below. This process was examined using two approaches.

First, changes in mixed-layer bSi concentration within SCW due to detrainment were estimated by combining vertical gradients in bSi concentration with storm-forced changes in the depth of the mixed layer following Johnson et al. (2024) (see Text S5a in Supporting Information S1). Detrainment during storm events decreased the average mixed-layer bSi concentration by 0.03–0.3 µM (Figure 11a) and accounted for 47% of the observed decline in bSi concentration in the mixed layer over the course of the cruise (Figure 11b). The remaining decrease was likely driven by lateral advection together with gravitational sinking losses.

The second approach evaluated the amount of bSi isolated below the mixed layer by the mixed-layer pump. An event of this type was defined as beginning when a given mixing event produced its deepest mixed layer, Z_{max}. The event progresses with re-stratification and ends when the next mixing event drives the depth of the mixed layer depth back to Z_{max} (Figure S5 in Supporting Information S1). The average thickness of the depth interval isolated between the base of the mixed layer associated with restratification and Z_{max} was calculated for each event (see Text S5b in Supporting Information S1). That calculation showed that events associated with the first three storms isolated layers with an average thickness of 10–40 m with that value increasing to 70–90 m as a result of the fourth storm (Figure 8).

The inventory of bSi within the layers of water isolated below the mixed layer was calculated for each event (see Text S5b in Supporting Information S1). The amount of bSi isolated during events ranged from 19.5 to 29.3 mmol Si m^{-2} across the three epochs (Table 6). The potential for the isolated particles of bSi to contribute to the observed rates of bSi export was assessed by comparing the average integrated bSi within the isolated layers, $\int \overline{bSi_{iso}}$, and bSi export rates measured just below the euphotic zone using data from both sediment traps and ^{234}Th (Table 5). Normalizing $\int \overline{bSi_{iso}}$, to the corresponding rate of export yields a conservatively short turnover time for detrained bSi as it assumes that only detrained bSi contributes to bSi export flux. Assuming that the

Table 6
The Amount of bSi Isolated Below the Mixed Layer, $\int \overline{bSi_{iso}}$, and the Duration of Isolation Compared to bSi Export Across the Three Epochs

Epoch	Epoch duration (d)	$\int \overline{bSi_{iso}}$ (mmol Si m^{-2})	Average time detrained particles spent below ML (d)	Turnover time of detrained particles (d)		Maximum contribution to export (%)	
				Traps	^{234}Th	Traps	^{234}Th
1	6	23.2 ± 10.7	1.3 ± 0.9	23.2 ± 10.7	6.4 ± 3.3	336 ± 156	107 ± 55
2	9	29.3 ± 3.2	1.4 ± 0.9	11.7 ± 1.6	9.2 ± 1.5	130 ± 18	102 ± 17
3	8	19.5 ± 9.4	2.0 ± 1.0	3.4 ± 1.6	3.3 ± 1.6	42 ± 21	41 ± 20

Note. Turnover times of detrained bSi is estimated as $\int \overline{bSi_{iso}}$ normalized to the bSi export rates for each epoch from Table 5. The maximum contribution of $\int \overline{bSi_{iso}}$ to export is computed as [$\int \overline{bSi_{iso}}$ ÷ (average bSi export rate × epoch duration)] × 100. Uncertainty terms are standard deviations.

measured rates of bSi export were sustained over the entire duration of each epoch, comparison of the calculated turnover times to the duration of each epoch indicates that detrained bSi could potentially support all of the measured bSi export during epochs 1 and 2 (turnover time > epoch duration) but not during epoch 3 (turnover time < epoch duration). To look at the same data from a different perspective the maximum contribution of detrained bSi to export was calculated as [$\int \overline{bSi_{iso}}$ ÷ (average bSi export rate × epoch duration)] × 100. The bSi within the isolated layers could support all of the bSi flux measured using both sediment traps and ^{234}Th during epochs 1 and 2 (Table 6). During epoch 3, when export flux increased (Table 5), the fraction of export that could potentially be supported by the sinking of isolated bSi dropped to 41%–42%. Thus, surface dynamics that isolated bSi below the mixed layer may have played a significant role in bSi export during epochs 1 and 2 when bSi export was more modest, but this mechanism cannot explain the significant increase in bSi export during epoch 3.

Mixed-layer dynamics combined with other export pathways also resulted in a progressive shift in the bSi inventory to deeper depths in the upper 500 m over time. The fraction of bSi in the upper 125 m that was present below the mixed layer initially declined during epoch 1 but then rose through epochs 2 and 3 (Figure 12a), implying a shift in the distribution of bSi to deeper depths within the upper 125 m. Simultaneously, there was a general loss of bSi from the upper 125 m during epochs 2 and 3 (Figures 3b and 12b). Data from deeper in the upper mesopelagic suggest that gravitational sinking contributed to that decline. Concentrations of bSi increase with time between 125 and 500 m, but the increase is attenuated with depth (Figure 12c). It appears that the influence of storms combined with persistent silicon limitation truncated silica production to where its loss due to dissolution and export outpaced its production, thus allowing bSi to be drained from surface waters through the combined action of the biological and physical pumps.

5. Conclusions

The EXPORTS North Atlantic expedition sampled a retentive eddy after the main diatom-phase of the spring bloom. Silicic acid limitation of silica production was initially sufficiently severe to imply growth limitation of diatoms by silicic acid. A series of four storms over the next 3.5 weeks entrained silicic acid into the mixed layer partially relieving, but not eliminating, Si limitation. Silica production was overwhelmingly dominated by the large size fraction, although V_b was highest in the small size fraction over most of the cruise, which is tentatively attributed to the activity of small diatoms. The inventory of bSi in surface waters was initially fairly high, but it declined over the cruise in concert with reductions in chlorophyll *a* and a shift to phytoplankton taxa other than diatoms. Silica production rates were intermediate compared with measurements from past studies examining the Northeast Atlantic during spring, consistent with sampling the remnant of a large diatom bloom that ended prior to the cruise.

The resupply of silicic acid via entrainment during storms coupled with relatively high rates of silica dissolution in the euphotic zone allowed significant silica production to continue following initial silicic acid depletion, such that post-diatom bloom integrated silica production summed over the entire cruise was 32% of that estimated during the main diatom bloom event. Estimated losses due to silica dissolution in the euphotic zone were higher than the global average, consistent with the increase in D:P typically associated with post-bloom periods. Somewhat surprisingly, diatoms contributed significantly to both new and primary production after the initial bloom, possibly dominating both. Their contribution to POC export was also significant. In general, the results are consistent with the initial diatom phase of the North Atlantic bloom terminating due to exhaustion of silicic acid

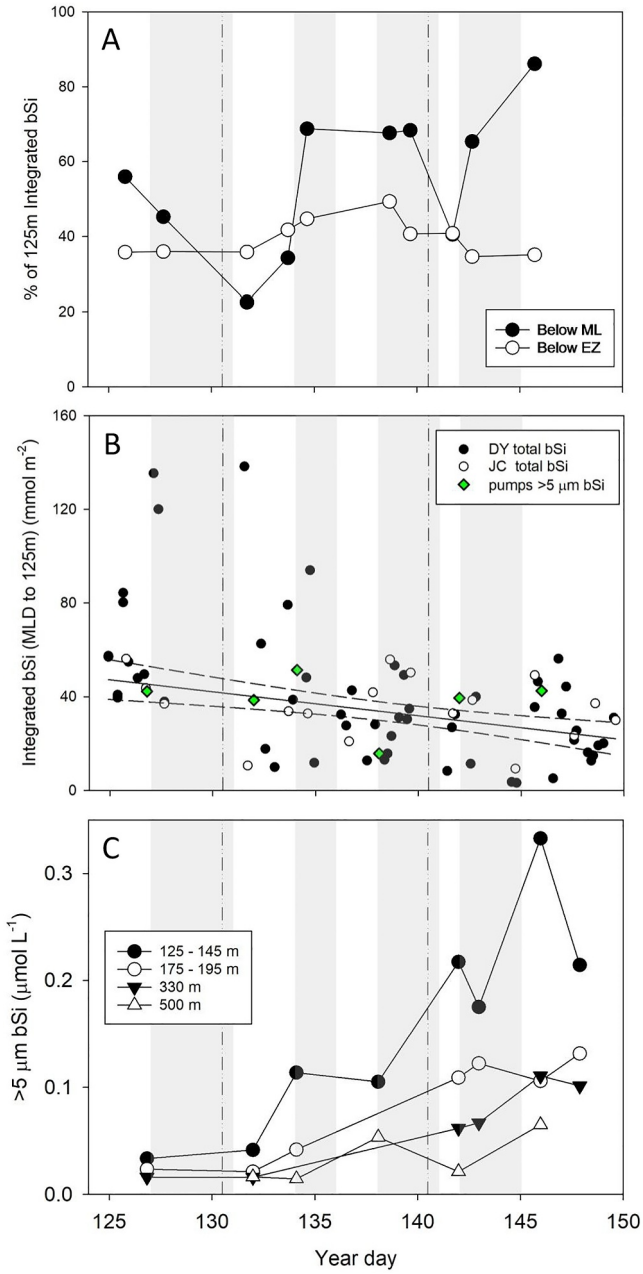

Figure 12. Time courses of (a) the fraction of biogenic silica present in the upper 125 m that was below the euphotic zone (EZ) and below the mixed layer (ML) in surface core waters. (b) Integrated biogenic silica concentration from the base of the mixed layer to 125 m for measurements from CTD casts and from in situ pumps. Filled and open circles represent data from CTD casts by *Discovery* (DY) and *James Cook* (JC), respectively. Green diamonds are >5 µm bSi from in situ pumps (Clevenger et al., 2024). (c) Biogenic silica concentrations in >5 µm particles at various depth intervals sampled by in situ pumps (Clevenger et al., 2024). Vertical gray bars indicate time periods associated with storms and vertical lines define boundaries between epochs, as defined by Johnson et al. (2024).

with sustained net silica production transitioning to reliance on silica dissolution and physical entrainment that replenish silicic acid in the mixed layer. The extent of the post-bloom silica production will depend on the frequency and efficiency of silicic-acid entrainment events and can persist longer than observed here, at least until the more abundant nitrate is exhausted through use by both diatoms and non-siliceous phytoplankton.

Data Availability Statement

All NSF-funded EXPORTS data used in this report are archived at the Biological and Chemical Oceanography Data Management Office under Brzezinski et al. (2023). All NASA-funded EXPORTS data are archived at NASA's SeaWiFS Bio-optical Archive and Storage System (SeaBASS) under Behrenfeld et al. (2021).

Acknowledgments

Support was provided through the National Science Foundation Biological Oceanography program and the NASA Ocean Biology and Biogeochemistry program. We greatly acknowledge the cooperation, skill and commitment of the Captains, Crews, Research Technicians and Administrative Staffs of the RRS *James Cook* (JC214), RRS *Discovery* (DY131) for making the EXPORTS North Atlantic field deployment a success. The EXPORTS program is funded by the NASA Ocean Biology and Biogeochemistry program with contributions from the U.S. National Science Foundation. In particular, MAB, KNB, BDJ, and JLJ were funded through NSF Grants NSF-OCE 1756442 (MAB, JLJ), NSF-OCE 1756433 (KNB), NSF-OCE 1756816 (BDJ). LJ was funded through NASA Grant 80NSSC17K0663. ER was funded through NASA Grant 80NSSC17K0692. M-R-M and SC were supported by NASA Grant NSSC17K0555. MR-M was also supported by funding from the Ocean Frontier Institute International Postdoctoral Fellowship Program and the Beatriu de Pinós Postdoctoral Program (2021-BP-00109). ME was supported by NASA Grants 80NSSC17K0662 and 80NSSC21K0015.

References

Alkire, M., D'Asaro, E., Lee, C., Jane Perry, M., Gray, A., Cetinić, I., et al. (2012). Estimates of net community production and export using high-resolution, Lagrangian measurements of O_2, NO_3^-, and POC through the evolution of a spring diatom bloom in the North Atlantic. *Deep Sea Research Part I: Oceanographic Research Papers*, *64*, 157–174. https://doi.org/10.1016/j.dsr.2012.01.012

Allen, J. T., Brown, L., Sanders, R., Mark Moore, C., Mustard, A., Fielding, S., et al. (2005). Diatom carbon export enhanced by silicate upwelling in the northeast Atlantic. *Nature*, *437*(7059), 728–732. https://doi.org/10.1038/nature03948

Baines, S. B., Twining, B. S., Brzezinski, M. A., Krause, J. W., Vogt, S., Assael, D., & McDaniel, H. (2012). Significant silicon accumulation by marine picocyanobacteria. *Nature Geoscience*, *5*(12), 886–891. https://doi.org/10.1038/ngeo1641

Becker, S., Aoyama, M., Woodward, E. M. S., Bakker, K., Coverly, S., Mahaffey, C., & Tanhua, T. (2020). GO-SHIP repeat hydrography nutrient manual: The precise and accurate determination of dissolved inorganic nutrients in seawater, using continuous flow analysis methods. *Frontiers in Marine Science*, *7*. https://doi.org/10.3389/fmars.2020.581790

Behrenfeld, M., Benitez-Nelson, C., Boss, E., Bourdin, G., Brzezinski, M., Buesseler, K., et al. (2021). Exports [Dataset]. *SeaWiFS Bio-optical Archive and Storage System (SeaBASS), NASA*. https://doi.org/10.5067/SeaBASS/EXPORTS/DATA001

Behrenfeld, M. J. (2010). Abandoning Sverdrup's critical depth hypothesis on phytoplankton blooms. *Ecology*, *91*(4), 977–989. https://doi.org/10.1890/09-1207.1

Behrenfeld, M. J., Doney, S. C., Lima, I., Boss, E. S., & Siegel, D. A. (2013). Annual cycles of ecological disturbance and recovery underlying the subarctic Atlantic spring plankton bloom. *Global Biogeochemical Cycles*, *27*(2), 526–540. https://doi.org/10.1002/gbc.20050

Billett, D. S. M., Lampitt, R. S., Rice, A. L., & Mantoura, R. F. C. (1983). Seasonal sedimentation of phytoplankton to the deep-sea benthos. *Nature*, *302*(5908), 520–522. https://doi.org/10.1038/302520a0

Binetti, U., Kaiser, J., Damerell, G. M., Rumyantseva, A., Martin, A. P., Henson, S., & Heywood, K. J. (2020). Net community oxygen production derived from Seaglider deployments at the Porcupine Abyssal Plain site (PAP; northeast Atlantic) in 2012-13. *Progress in Oceanography*, *183*, 102293. https://doi.org/10.1016/j.pocean.2020.102293

Brown, L., Sanders, R., Savidge, G., & Lucas, C. H. (2003). The uptake of silica during the spring bloom in the northeast Atlantic Ocean. *Limnology & Oceanography*, *48*(5), 1831–1845. https://doi.org/10.4319/lo.2003.48.5.1831

Brzezinski, M. A. (1985). The Si-C-N ratio of marine diatoms—Interspecific variability and the effect of some environmental variables. *Journal of Phycology*, *21*(3), 347–357. https://doi.org/10.1111/j.0022-3646.1985.00347.x

Brzezinski, M. A., Buck, K., & Jenkins, B. D. (2023). Depth profiles in the euphotic zone of nitrate, silicate, and phosphate concentrations and profiles of silicic acid uptake rates from EXPORTS cruise DY131 in the North Atlantic during May 2021. Biological and Chemical Oceanography Data Management Office (BCO-DMO). (Version 1). Version Date 2023-04-12 [Dataset]. *BCO DMO*. https://doi.org/10.26008/1912/BCO-DMO.893293.1

Brzezinski, M. A., Jones, J. L., Bidle, K. D., & Azam, F. (2003). The balance between silica production and silica dissolution in the sea: Insights from Monterey Bay, California, applied to the global data set. *Limnology & Oceanography*, *48*(5), 1846–1854. https://doi.org/10.4319/lo.2003.48.5.1846

Brzezinski, M. A., & Phillips, D. R. (1997). Evaluation of ^{32}Si as a tracer for measuring silica production rates in marine waters. *Limnology & Oceanography*, *42*(5), 856–865. https://doi.org/10.4319/lo.1997.42.5.0856

Brzezinski, M. A., Varela, D. E., Jenkins, B. D., Buck, K. N., Kafrissen, S. M., & Jones, J. L. (2022). The upper ocean silicon cycle of the subarctic Pacific during the EXPORTS field campaign. *Elementa: Science of the Anthropocene*, *10*(1), 00087. https://doi.org/10.1525/elementa.2021.00087

Buesseler, K. O., & Boyd, P. W. (2009). Shedding light on processes that control particle export and flux attenuation in the twilight zone of the open ocean. *Limnology & Oceanography*, *54*(4), 1210–1232. https://doi.org/10.4319/lo.2009.54.4.1210

Clevenger, S. J., Benitez-Nelson, C. R., Roca-Martí, M., Bam, W., Estapa, M., Kenyon, J. A., et al. (2024). Carbon and silica fluxes during a declining North Atlantic spring bloom as part of the EXPORTS program. *Marine Chemistry*, *258*, 104346. https://doi.org/10.1016/j.marchem.2023.104346

Closset, I., Lasbleiz, M., Leblanc, K., Quéguiner, B., Cavagna, A. J., Elskens, M., et al. (2014). Seasonal evolution of net and regenerated silica production around a natural Fe-fertilized area in the Southern Ocean estimated with Si isotopic approaches. *Biogeosciences*, *11*(20), 5827–5846. https://doi.org/10.5194/bg-11-5827-2014

Dall'Olmo, G., Dingle, J., Polimene, L., Brewin, R. J. W., & Claustre, H. (2016). Substantial energy input to the mesopelagic ecosystem from the seasonal mixed-layer pump. *Nature Geoscience*, *9*(11), 820–823. https://doi.org/10.1038/ngeo2818

De La Rocha, C. L., & Passow, U. (2004). Recovery of *Thalassiosira weissflogii* from nitrogen and silicon starvation. *Limnology & Oceanography*, *49*(1), 245–255. https://doi.org/10.4319/lo.2004.49.1.0245

Durkin, C. A., Cetinić, I., Estapa, M., Ljubešić, Z., Mucko, M., Neeley, A., & Omand, M. (2022). Tracing the path of carbon export in the ocean though DNA sequencing of individual sinking particles. *The Isme Journal*, *16*(8), 1896–1906. https://doi.org/10.1038/s41396-022-01239-2

Enriquez, R. M., & Taylor, J. R. (2015). Numerical simulations of the competition between wind-driven mixing and surface heating in triggering spring phytoplankton blooms. *ICES Journal of Marine Science*, *72*(6), 1926–1941. https://doi.org/10.1093/icesjms/fsv071

Erickson, Z. K., Fields, E., Johnson, L., Thompson, A. F., Dove, L. A., D'Asaro, E., & Siegel, D. A. (2023). Eddy tracking from in situ and satellite observations. *Journal of Geophysical Research: Oceans*, *128*(8), e2023JC019701. https://doi.org/10.1029/2023JC019701

Estapa, M., Buesseler, K., Durkin, C. A., Omand, M., Benitez-Nelson, C. R., Roca-Martí, M., et al. (2021). Biogenic sinking particle fluxes and sediment trap collection efficiency at Ocean Station Papa. *Elementa: Science of the Anthropocene*, *9*(1). https://doi.org/10.1525/elementa.2020.00122

Estapa, M., Valdes, J., Tradd, K., Sugar, J., Omand, M., & Buesseler, K. (2020). The neutrally buoyant sediment trap: Two decades of progress. *Journal of Atmospheric and Oceanic Technology*, *37*(6), 957–973. https://doi.org/10.1175/JTECH-D-19-0118.1

Estapa, M. L., Durkin, C. A., Slade, W. H., Huffard, C. L., O'Neill, S. P., & Omand, M. M. (2024). A new, global optical sediment trap calibration. *Limnology and Oceanography: Methods*, *22*(2), 77–92. https://doi.org/10.1002/lom3.10592

Gardner, W. D., Chung, S. P., Richardson, M. J., & Walsh, I. D. (1995). The oceanic mixed-layer pump. *Deep Sea Research Part II: Topical Studies in Oceanography*, *42*(2), 757–775. https://doi.org/10.1016/0967-0645(95)00037-Q

Hartman, S. E., Bett, B. J., Durden, J. M., Henson, S. A., Iversen, M., Jeffreys, R. M., et al. (2021). Enduring science: Three decades of observing the northeast Atlantic from the Porcupine Abyssal Plain Sustained Observatory (PAP-SO). *Progress in Oceanography*, *191*, 102508. https://doi.org/10.1016/j.pocean.2020.102508

Hátún, H., Azetsu-Scott, K., Somavilla, R., Rey, F., Johnson, C., Mathis, M., et al. (2017). The subpolar gyre regulates silicate concentrations in the North Atlantic. *Scientific Reports*, *7*(1), 14576. https://doi.org/10.1038/s41598-017-14837-4

Henson, S., Lampitt, R., & Johns, D. (2012). Variability in phytoplankton community structure in response to the North Atlantic Oscillation and implications for organic carbon flux. *Limnology & Oceanography*, *57*(6), 1591–1601. https://doi.org/10.4319/lo.2012.57.6.1591

Honjo, S., & Manganini, S. J. (1993). Annual biogenic particle fluxes to the interior of the North Atlantic Ocean; studied at 34°N 21°W and 48°N 21°W. *Deep Sea Research Part II: Topical Studies in Oceanography*, *40*(1–2), 587–607. https://doi.org/10.1016/0967-0645(93)90034-k

Johnson, L., Siegel, D. A., Thompson, A. F., Fields, E., Erickson, Z. K., Cetinic, I., et al. (2024). Assessment of oceanographic conditions during the North Atlantic EXport Processes in the Ocean from RemoTe Sensing (EXPORTS) field campaign. *Progress in Oceanography*, *220*, 103170. https://doi.org/10.1016/j.pocean.2023.103170

Krause, J. W., Brzezinski, M. A., & Jones, J. L. (2011). Application of low-level beta counting of Si for the measurement of silica production rates in aquatic environments. *Marine Chemistry*, *127*(1–4), 40–47. https://doi.org/10.1016/j.marchem.2011.07.001

Krause, J. W., Nelson, D. M., & Lomas, M. W. (2009). Biogeochemical responses to late-winter storms in the Sargasso Sea, II: Increased rates of biogenic silica production and export. *Deep-Sea Research Part I-Oceanographic Research Papers*, *56*(6), 861–874. https://doi.org/10.1016/j.dsr.2009.01.002

Krause, J. W., Schulz, I. K., Rowe, K. A., Dobbins, W., Winding, M. H. S., Sejr, M. K., et al. (2019). Silicic acid limitation drives bloom termination and potential carbon sequestration in an Arctic bloom. *Scientific Reports*, *9*(1), 8149. https://doi.org/10.1038/s41598-019-44587-4

Leblanc, K., Leynaert, A., Fernandez, C., I., Rimmelin, P., Moutin, T., Raimbault, P., et al. (2005). A seasonal study of diatom dynamics in the North Atlantic during the POMME experiment (2001): Evidence for Si limitation of the spring bloom. *Journal of Geophysical Research*, *110*(C7), C07S14. https://doi.org/10.1029/2004JC002621

Leblanc, K., Quéguiner, B., Diaz, F., Cornet, V., Michel-Rodriguez, M., Durrieu de Madron, X., et al. (2018). Nanoplanktonic diatoms are globally overlooked but play a role in spring blooms and carbon export. *Nature Communications*, *9*(1), 953. https://doi.org/10.1038/s41467-018-03376-9

Liu, H. B., Chen, M. R., Zhu, F., & Harrison, P. J. (2016). Effect of diatom silica content on copepod grazing, growth and reproduction. *Frontiers in Marine Science*, *3*. https://doi.org/10.3389/fmars.2016.00089

Lochte, K., Ducklow, H. W., Fasham, M. J. R., & Stienen, C. (1993). Plankton succession and carbon cycling at 47°N 20°W during the JGOFS North Atlantic bloom experiment. *Deep Sea Research Part II: Topical Studies in Oceanography*, *40*(1), 91–114. https://doi.org/10.1016/0967-0645(93)90008-B

Martin, P., Lampitt, R. S., Jane Perry, M., Sanders, R., Lee, C., & D'Asaro, E. (2011). Export and mesopelagic particle flux during a North Atlantic spring diatom bloom. *Deep Sea Research Part I: Oceanographic Research Papers*, *58*(4), 338–349. https://doi.org/10.1016/j.dsr.2011.01.006

Martin-Jézéquel, V., Hildebrand, M., & Brzezinski, M. A. (2000). Silicon metabolism in diatoms: Implications for growth. *Journal of Phycology*, *36*(5), 821–840. https://doi.org/10.1046/j.1529-8817.2000.00019.x

Meyer, M. G., Brzezinski, M. A., Cohn, M. R., Kramer, S. J., Paul, N., Sharpe, G., et al. (2023). Primary production dynamics during the decline phase of the North Atlantic annual spring bloom. *bioRxiv*. https://doi.org/10.1101/2023.05.18.541304

Ohnemus, D. C., Rauschenberg, S., Krause, J. W., Brzezinski, M. A., Collier, J. L., Geraci-Yee, S., et al. (2016). Silicon content of individual cells of Synechococcus from the North Atlantic Ocean. *Marine Chemistry*, *187*, 16–24. https://doi.org/10.1016/j.marchem.2016.10.003

Paasche, E. (1973). Silicon and the ecology of marine plankton diatoms. I. *Thalassiosira pseudonana* (*Cyclotella nana*) grown in a chemostat with silicate as limiting nutrient. *Marine Biology*, *19*(2), 117–126. https://doi.org/10.1007/BF00353582

Poulton, A. J., Sanders, R., Holligan, P. M., Stinchcombe, M. C., Adey, T. R., Brown, L., & Chamberlain, K. (2006). Phytoplankton mineralization in the tropical and subtropical Atlantic Ocean. *Global Biogeochemical Cycles*, *20*(4). https://doi.org/10.1029/2006GB002712

Ragueneau, O., Laynaert, A., Treguer, P., Nelson, D. M., Fischer, G., DeMaster, D. J., et al. (1997). OPALEO (OPAL as PALEO-productivity proxy). Synthesis and perspectives Report.

Ragueneau, O., & Tréguer, P. (1994). Determination of biogenic silica in coastal waters: Applicability and limits of the alkaline digestion method. *Marine Chemistry*, *45*(1–2), 43–51. https://doi.org/10.1016/0304-4203(94)90090-6

Romanelli, E., Giering, S. L. C., Siegel, D. A., & Passow, U. (2024). Intense storms affect sinking particle fluxes after the North Atlantic diatom spring bloom. *bioRxiv*. https://doi.org/10.1101/2024.01.11.575202

Rumyantseva, A., Henson, S., Martin, A., Thompson, A. F., Damerell, G. M., Kaiser, J., & Heywood, K. J. (2019). Phytoplankton spring bloom initiation: The impact of atmospheric forcing and light in the temperate North Atlantic Ocean. *Progress in Oceanography*, *178*, 102202. https://doi.org/10.1016/j.pocean.2019.102202

Ryderheim, F., Grønning, J., & Kiørboe, T. (2022). Thicker shells reduce copepod grazing on diatoms. *Limnology and Oceanography Letters*, *7*(5), 435–442. https://doi.org/10.1002/lol2.10243

Sarmiento, J. L., Gruber, N., Brzezinski, M. A., & Dunne, J. P. (2004). High-latitude controls of thermocline nutrients and low latitude biological productivity. *Nature*, *427*(6969), 56–60. https://doi.org/10.1038/nature02127

Savidge, G., Boyd, P., Pomroy, A., Harbour, D., & Joint, I. (1995). Phytoplankton production and biomass estimates in the northeast Atlantic Ocean, May–June 1990. *Deep Sea Research Part I: Oceanographic Research Papers*, *42*(5), 599–617. https://doi.org/10.1016/0967-0637(95)00016-Y

Siegel, D., Burd, A., Estapa, M., Fields, E., Johnson, L., Romanelli, E., et al. (2024). Dynamics of aggregates and sinking carbon fluxes in a turbulent ocean. *EarthArXiv*. https://doi.org/10.31223/X58709

Siegel, D. A., Cetinić, I., Graff, J. R., Lee, C. M., Nelson, N., Perry, M. J., et al. (2021). An operational overview of the EXport Processes in the Ocean from RemoTe Sensing (EXPORTS) Northeast Pacific field deployment. *Elementa: Science of the Anthropocene*, *9*(1). https://doi.org/10.1525/elementa.2020.00107

Sieracki, M. E., Verity, P. G., & Stoecker, D. K. (1993). Plankton community response to sequential silicate and nitrate depletion during the 1989 North-Atlantic spring bloom. *Deep-Sea Research II*, *40*(1–2), 213–225. https://doi.org/10.1016/0967-0645(93)90014-E

Thiel, H., Pfannkuche, O., Schriever, G., Lochte, K., Gooday, A. J., Hemleben, C., et al. (1989). Phytodetritus on the deep-sea floor in a central oceanic region of the northeast Atlantic. *Biological Oceanography*, *6*(2), 203–239. https://doi.org/10.1080/01965581.1988.10749527

Tréguer, P. J., Sutton, J. N., Brzezinski, M., Charette, M. A., Devries, T., Dutkiewicz, S., et al. (2021). Reviews and syntheses: The biogeochemical cycle of silicon in the modern ocean. *Biogeosciences*, *18*(4), 1269–1289. https://doi.org/10.5194/bg-18-1269-2021

Turner, J. (2002). Zooplankton fecal pellets, marine snow and sinking phytoplankton blooms. *Aquatic Microbial Ecology*, *27*, 57–102. https://doi.org/10.3354/ame027057

Waite, A. M., Olson, R. J., Dam, H. G., & Passow, U. (1995). Suger-containing compounds on the cell surfaces of marine diatoms measured using concanavalin A and flow cytometry. *Journal of Phycology*, *31*(6), 925–933. https://doi.org/10.1111/j.0022-3646.1995.00925.x